Research Square

Preprints are preliminary reports that have not undergone peer review.
They should not be considered conclusive, used to inform clinical practice,
or referenced by the media as validated information.

# The HYdroclimate Drought and Rainfall Atlas (HYDRA): A global atlas of hydroclimate variability linked to large-scale ocean-atmosphere climate modes

**Aandishah T. Samara**

aandishah.s@columbia.edu

Columbia University

**Richard Seager**

Lamont-Doherty Earth Observatory

**Jason E. Smerdon**

Columbia University

**data-descriptor**

**Keywords:**

**Posted Date:** November 24th, 2026

**DOI:** https://doi.org/10.21203/rs.3.rs-11322731/v1

**License:** This work is licensed under a Creative Commons Attribution 4.0 International License.
Read Full License

**Additional Declarations:** No competing interests reported.

# The HYdroclimate Drought and Rainfall Atlas (HYDRA): A global atlas of hydroclimate variability linked to large-scale ocean-atmosphere climate modes

Aandishah T. Samara[1,2,3] , Richard Seager[2], Jason E. Smerdon[3]

[1]Department of Earth and Environmental Sciences, Columbia University in the City of New York, New York, New York

[2]Lamont-Doherty Earth Observatory, Division of Ocean and Climate Physics, Columbia University, Palisades, New York

[3]Columbia Climate School, Columbia University, New York, New York

Corresponding Author: Aandishah T. Samara, aandishah.s@columbia.edu

**Abstract.** Global and regional hydroclimate variability is strongly modulated by large-scale ocean-atmosphere modes with variability on interannual to multidecadal timescales. Assessments of how these modes influence terrestrial hydroclimate, such as soil moisture, precipitation, and temperature, remain scattered across studies that differ in their employed datasets, the climate index definitions that quantify the modal states and the temporal periods chosen for analysis and defined climatologies. We present a systematized global archive of climate indices, teleconnection maps, and agreement composite analyses linking ten major climate indices to hydroclimate fields derived from observational and reanalysis products. The climate indices target ocean-based modes derived from sea surface temperatures (El Niño-Southern Oscillation, Pacific Decadal Oscillation, Atlantic Multidecadal Oscillation, Indian Ocean Dipole, and the Tripole Index) over the period 1902-2024, and atmospheric circulation-based modes derived from geopotential height and sea level pressure (Arctic Oscillation, Antarctic Oscillation, North Atlantic Oscillation, North Pacific Index, and Southern Annual Mode) over the period 1941-2024. All ten indices are also provided over a common short-term period (1981-2024). All assessments are provided over four seasonal windows (December-January-February, March-April-May, June-July-August, and September-October-November); all indices are computed with common data sets, climatological baselines, and temporal periods. This database, which we term the Hydrological Drought and Rainfall Atlas (HYDRA), is available on a web-based platform allowing exploration of large-scale drivers of global and regional hydroclimate variability. Collectively, HYDRA is an open and systematized resource for the research community that allows easy and consistent comparisons of climate variability across large-scale modes, variables, and seasons.

## 1. Background & Summary

Hydroclimate extremes, such as droughts and pluvials, are among the most consequential climate hazards globally, disrupting water availability, agricultural production, ecosystem stability, and human health worldwide (IPCC, 2023; WMO, 2023). These events ultimately arise from local

imbalances in precipitation (Swain et al., 2025; Trenberth et al., 1998, 2014; Zhao et al., 2022) and evapotranspiration, but can be driven by large-scale modes of variability that redistribute heat and moisture on timescales from seasons to decades (Deser et al., 2010; Özger et al., 2009; Trenberth et al., 1998). Understanding the spatial fingerprints of these climate modes on hydroclimate variables is therefore critical for interpreting past and future drought and pluvial variability (Cheung et al., 2025; Hoerling & Kumar, 2003; Kundzewicz et al., 2019; Mishra & Singh, 2010; Power et al., 2006; S. Schubert et al., 2009; Seager et al., 2023; Yeh et al., 2018). Additionally, human-driven climate change is causing droughts to intensify and develop more rapidly (AghaKouchak et al., 2021; Pendergrass et al., 2020; Yuan et al., 2023), raising regional drought risk (Williams et al., 2020, 2022; Yuan et al., 2019), amplifying precipitation extremes (Allan & Soden, 2008; Rodell & Li, 2023; S. Zhang et al., 2022) and causing shifts in the mean atmospheric circulation and hydrological cycle that also alter drought and pluvial risk (Grise et al., 2019; Mantsis & Clement, 2009; Seager et al., 2024; Taschetto et al., 2020). Disentangling the contributions of internal ocean-atmosphere variability and external forcing is essential for both attributing the causes of observed hydroclimate trends and for assessing the likelihood of future extremes under continued warming and natural variability (Deser et al., 2020; Lehner et al., 2018; Marvel et al., 2019; Seager et al., 2026; Thornton et al., 2014).

Surface heat fluxes, transport of heat by currents, turbulent vertical mixing, and variations in upper-ocean mixed layer depth are the primary physical mechanisms driving changes in SST that arise in coupled-ocean atmosphere variability (Buckley & Marshall, 2016; Cronin et al., 2019; Deser et al., 2010; Foltz et al., 2019; H. E. Phillips et al., 2021). As they change, often through irregular cycles that recur over several years or decades, modes of ocean-atmosphere variability drive variations in hydroclimate globally, including shifts in precipitation, streamflow, droughts, and floods (Dai & Wigley, 2000; Kundzewicz et al., 2019; Li et al., 2021, 2022; S. D. Schubert et al., 2016). For example, through shifts in the Walker circulation and tropical convection, El Niño (the positive phase of the El Niño-Southern Oscillation (ENSO)) dries the Indian subcontinent (Ashok & Saji, 2007; K. K. Kumar et al., 2006; Ummenhofer et al., 2011), Southeast Asia (Ju & Slingo, 1995; Juneng & Tangang, 2005; Villafuerte & Matsumoto, 2015), the Sahel (Giannini et al., 2003; Janicot et al., 2001), northern South America (Andreoli & Kayano, 2005; Tedeschi et al., 2013), and Australia (Chiew et al., 1998; Ma et al., 2023; Risbey et al., 2009), while bringing wet anomalies to the southwestern United States (Cayan et al., 1999), Central Asia (Z. Chen et al., 2022), southeastern South America (Cai et al., 2020), and the Horn of Africa (Alizadeh, 2024; Mason & Goddard, 2001; Ropelewski & Halpert, 1987). One mechanism for change is that tropospheric warming during El Niño weakens tropical precipitation and monsoons via increased tropospheric stability (Chiang & Sobel, 2002). La Niña largely reverses teleconnection impacts, enhancing rainfall over the Sahel (Biasutti, 2019), southern Africa (Reason & Rouault, 2002), and South/Southeast Asia (K. K. Kumar et al., 1999) and Australia (Risbey et al., 2009), while drying Central and eastern Asia (Wang et al., 2000), southeastern South America (Grimm et al., 2000; Grimm & Tedeschi, 2009), and southern North America (Cole et al., 2002).

In addition to coupled modes of variability like ENSO, there are modes that arise from internal atmospheric dynamics and do not explicitly involve ocean-atmosphere coupling, even though they can be excited by sea surface temperatures (SSTs) and other surface boundary forcing. These modes also impact hydroclimate. For example, the positive phase of the North Atlantic Oscillation (NAO) is associated with enhanced and northward-shifted westerlies across the North Atlantic that bring above-normal winter precipitation to northern Europe and suppress rainfall across the Mediterranean and North Africa (Hurrell, 1995; Hurrell et al., 2003, 2003; Seager et al., 2022), while opposite conditions tend to occur during its negative phase. These coupled and atmospheric teleconnections are individually well documented but characterizing them so that they are comparable across modes, variables, and regions depends on the consistency of the underlying indices and analyses.

Previous studies have shown the value of methodologically consistent and accessible reference products for climate indices. For ENSO, for instance, the choice of definition, base period, and input dataset alters which events are identified and how their teleconnections appear (Capotondi et al., 2015; Hanley et al., 2003; L'Heureux et al., 2024). For empirical orthogonal function (EOF)-based indices (e.g., Pacific Decadal Oscillation (PDO), NAO), the patterns of which depend on the analysis period and the domain of decomposition and methodology, the consistency challenge is even more acute (X. Chen & Wallace, 2015; Wills et al., 2018). In some cases, the need for consistent modal definitions has been standardized. For instance, the Climate Variability Diagnostics Package (CVDP) (A. Phillips et al., 2020) was built to compare modes across models and observations with uniform definitions and processing and is now a community standard for evaluating variability across CMIP model generations and large ensembles (Capotondi et al., 2020; Eyring et al., 2016; Fasullo et al., 2020; Maher et al., 2025). Efforts such as these nevertheless have been focused on the modes themselves, their indices, their SST and sea level pressure (SLP) signatures, and ultimately their fidelity in models. To our knowledge, no systematized assessment and reference dataset has been established for oceanic and atmospheric modes and their imprint on hydroclimate fields. Where such studies have been performed, they differ in which variables they examine, which observational products they draw upon, and over which intervals regressions are computed, leaving comparisons ambiguous as to whether differences in estimated hydroclimate teleconnection patterns are methodological or physical (Deser et al., 2017; Newman et al., 2016). What's missing is a database of modes of climate variability with associated hydroclimate teleconnections for precipitation, temperature, drought severity and soil moisture that allows easy comparison across modes, seasons and time intervals.

To address this gap, we introduce the HYdrological Drought and Rainfall Atlas (HYDRA) database that comprises ten major ocean and atmospheric climate indices, and associated hydroclimate teleconnection patterns, defined over common climatological periods using consistent input datasets and processing choices for both longer and shorter intervals. SST is used to derive five ocean-based indices: ENSO (Rayner et al., 2003; Trenberth, 1997), the PDO (Mantua et al., 1997; Newman et al., 2016), the Atlantic Multidecadal Oscillation (AMO) (Enfield et al.,

2001a), the Indian Ocean Dipole (IOD) (Saji et al., 1999), and the Tripole Index (TPI) (Henley et al., 2015). The remaining five indices are derived from large-scale atmospheric fields: geopotential height (HGT) is used to define the Arctic Oscillation (AO) (Thompson & Wallace, 1998, 2000) and Antarctic Oscillation (AAO) (Mo, 2000), while SLP fields are used to describe the NAO (Hurrell, 1995), the North Pacific Index (NPI) (Trenberth & Hurrell, 1994), and the Southern Annular Mode (SAM)(Gong & Wang, 1999) .

Using the indices derived from our systematized calculations, we generate seasonal regression maps and agreement composites for major hydroclimate variables, including the Palmer Drought Severity Index (PDSI), soil moisture, precipitation, and surface air temperature. Across four seasons, this framework characterizes where the influences of climate modes leave spatial fingerprints of dryness, wetness, and temperature. Because the input fields for the ocean and atmospheric circulation-based indices have different historical coverage, HYDRA is developed for three standard analysis periods based on dataset availability: a long-term period (LT, 1902-2024) for SST-based indices computed from HadISST 1.1 (Rayner et al., 2003), an intermediate period (IT, 1941-2024) for HGT and SLP-based indices computed from ERA5 (Bell et al., 2021; Hersbach et al., 2020), and a common short-term period (ST, 1981-2024) encompassing all ten indices together with the hydroclimate fields. For each index and analysis period, HYDRA provides the index time series, gridded seasonal hydroclimate teleconnection maps and agreement composites, along with accompanying significance and agreement masks. These products are freely available for download through the HYDRA website. The product is designed to serve as an open resource for the climate research community that can be used for the easy, convenient, consistent and comparative assessment of modes of climate variability and their hydroclimate impacts.

## 2. Methods

To characterize large-scale climate variability and its influence on hydroclimate fields, HYDRA has been developed using an open-source, standardized framework for computing climate indices and their influence on terrestrial hydroclimate. HYDRA ensures that index definitions, and computation methods are applied uniformly across datasets, removing inconsistencies that commonly arise when indices are recalculated using different conventions, software implementations or different reference intervals. Building on these indices, we create teleconnection maps that quantify the statistical association between each climate index and hydroclimate variable of interest (e.g., precipitation, surface temperature, soil moisture) across the study domain. These maps are produced using a consistent processing pipeline across all climate indices to help enable direct comparison of teleconnection patterns across different datasets, spatial resolutions, and time periods. The datasets and methods used in this study are summarized in Figure 1, which outlines the computation, validation, and structure of the HYDRA dataset.

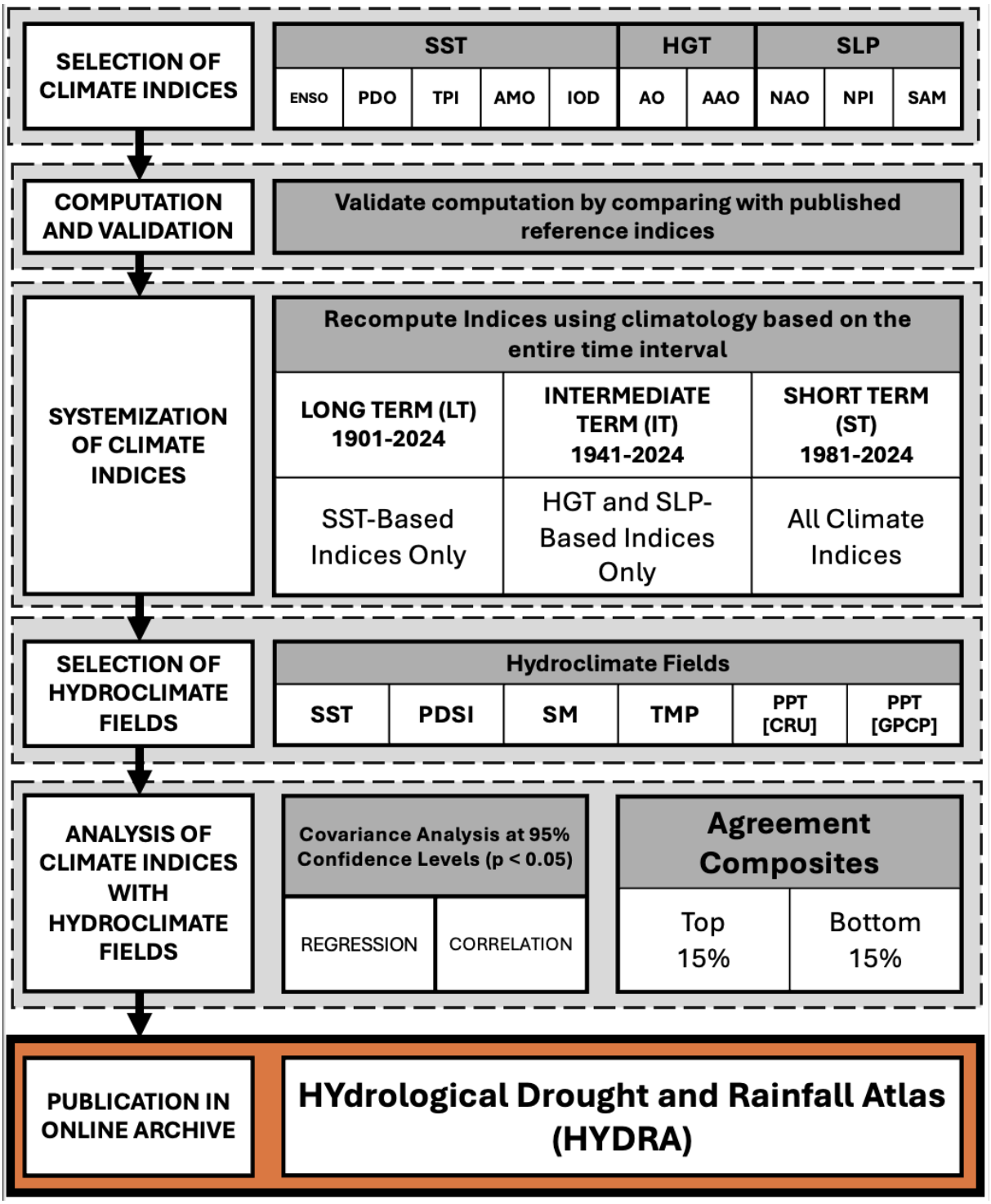



***Figure 1****. Flowchart showing each of the data processing steps for the production of HYDRA.*

HYDRA is intended as a dynamic working resource rather than an additional set of stationary datasets. In this study, the SST-based indices are derived from HADISST 1.1 and the atmospheric

indices are computed from ERA5. However, the workflow is not tied to these products. Users can substitute other SST datasets in place of HADISST 1.1, or any other atmospheric fields and products for the circulation-based indices. Differences between SST products have been found due to the differences in their input data, bias adjustments, and interpolation methods, especially for data-sparse regions and time periods (Chan et al., 2026). As such, HYDRA provides reproducible code that can be applied to any gridded hydroclimate product and any user-defined analysis period and baseline to help support future assessments and updates as new datasets become available. This helps to ensure methodological transparency and reproducibility so that all index and hydroclimate teleconnection patterns follow the same documented workflow regardless of the input data source.

### a. Input datasets

All input datasets used to compute the climate indices were obtained from publicly accessible repositories and are summarized in Table 1. The LT and ST hydroclimate variables are from the Climate Research Unit Time Series version 4.08 (CRU TS v4.09) (Harris et al., 2020), which includes precipitation, temperature, and PDSI (van der Schrier et al., 2011, 2013) from 1902 to 2024. SSTs are taken from the Hadley Centre Sea Ice and SST dataset version 1.1 that covers the period 1871 to 2024. For the IT and ST periods, HGT and SLP are from the European Centre for Medium-Range Weather Forecasts ERA5 reanalysis (Bell et al., 2021; Hersbach et al., 2020) that covers the period 1940 to recent. Table 1 also summarizes hydroclimate variables that are employed for estimation of teleconnection patterns discussed subsequently in this data product report. For the ST period, soil moisture is taken from the Global Land Evaporation Amsterdam Model version 4.2a (GLEAM v4.2a) (Miralles et al., 2025) and precipitation over land and ocean from the Global Precipitation Climatology Project monthly analysis, version 2.3 (GPCP v2.3) (Adler et al., 2003) that combines satellite and gauge data. The data availability of these various datasets determines the LT, IT and ST start dates as 1902, 1941, and 1981, respectively.

**Table 1.** All datasets used in the production of HYDRA.

| Variable | Dataset | Temporal Coverage | Spatial Coverage | Resolution | Reference |
|---|---|---|---|---|---|
| Sea surface temperature (SST) | HadISST v1.1 | 1902-2024 | Global Ocean | 1° | Rayner et al. (2003) |
| Geopotential Height (HGT) | ERA5 | 1941-2024 | Global Land and Ocean | 0.25° | Hersbach et al., 2023 |

| | | | | | |
|---|---|---|---|---|---|
| Sea Level Pressure (SLP) | ERA5 | 1941-2024 | Global Ocean | 0.25 ° | Hersbach et al., 2023 |
| Palmer Drought Severity Index (PDSI) | scPDSI v4.09 | 1902-2024 | Global Land only | 0.5 ° | Barichivich et al. (2024) |
| Precipitation (PPT_CRU) | CRU TS v4.09 | 1902-2024 | Global Land only | 0.5 ° | Harris et al. (2020) |
| Precipitation (PPT_GPCP) | GPCP v2.3 | 1981-2024 | Global Land and Ocean | 1 ° | Adler et al. (2003) |
| 2-m Surface Air Temperature (TMP) | CRU TS v4.09 | 1902-2024 | Global Land only | 0.5 ° | Harris et al. (2020) |
| Rootzone Soil moisture (SM) | GLEAM v4.2a | 1981-2024 | Global Land only | 0.25 ° | Martens et al. (2017) |

### b. Validation and Systemization of Climate Indices

We focus on ten of the most widely used climate indices derived from ocean and atmospheric circulation fields (Barnston & Livezey, 1987; Deser et al., 2010; Norel et al., 2021), which also have well-established influences on hydroclimate variability (Ashok et al., 2001; Fogt & Marshall, 2020; Gillett et al., 2006; He et al., 2026; Kundzewicz et al., 2019; Liu et al., 2021; McCabe et al., 2004). Using the published definitions of these indices, each was independently validated against externally published index values (see Table 2) before being recomputed from consistent gridded SST and reanalysis datasets. The result is a curated collection of climate indices that can be used consistently for intercomparison, rather than relying on externally published values computed from differing source data, methods, time periods, or reference intervals.

The five ocean-based indices (ENSO, PDO, AMO, IOD, and TPI) were computed using SSTs from HadISST 1.1 and are available for the LT and ST periods. The five atmospheric circulation-based indices (AO, AAO, SAM, NAO, NPI) were computed from ERA5 HGT and SLP fields over the IT and ST periods. The ST period is the only time interval over which all ten indices are available. Start dates for the LT and IT periods were set by the longest record available for each respective dataset, while the ST period was additionally chosen both to provide a common interval

across all ten indices and to align with the satellite era, over which some underlying data (e.g. ERA5 Reanalysis) are most reliable.

All indices were computed on a monthly basis and then aggregated to seasonal means for the four standard seasons: December-February (DJF), March-May (MAM), June-August (JJA), and September-November (SON). All systematized indices are shown for the LT, IT and ST periods in Figure 2.

Table 2 summarizes the definitions of the ten HYDRA climate indices that are produced in this data product. The table also includes the source, citation, and datasets used to derive the publicly available versions of the indices, the time period over which each index is available (termed the reference period), and the time period used as the baseline climatology for the index calculations, if applicable. For validation against published indices, each index in our data product was computed using the same input data, time period, methodology and base climatology as the reference (see Technical Validation section). After validation against the published indices, we construct systemized versions of each index using the same methodology employed in our validation exercises, but the new indices are computed using consistent datasets, time periods, and climatological baselines for a common framework across the HYDRA products.

**Table 2.** Definitions of the 10 modal indices computed in this data product. Also listed are the independently published indices and their original input datasets, the latter of which are used to validate the index calculations performed in this study. Following validation, all indices computed in this study use the datasets detailed in Table 1.

| Index | Full name | Definition | Ref. for Validation | Val. Period | Ref. Baseline Period | Citation |
|---|---|---|---|---|---|---|
| ENSO | El Nino-Southern Oscillation | Area averaged SST anomalies over the Niño 3.4 region (5N-5S) (170-120W) | NOAA Niño 3.4 SST Index from HadISST1.1 | 1902-2024 | 1981-2010 | Rayner et al., 2003, Trenberth et al., (1997) |
| PDO | Pacific Decadal Oscillations (or Variability) | Leading EOF of monthly SST anomalies in the North Pacific (20N-70N) with the global mean removed | NOAA PDO (or PDV) from HadISST1.1 | 1902-2024 | 1920-2014 | Mantua et al., (1997) |
| AMO | Atlantic Multidecadal Oscillations (or Variability) | Area weighted average over the SST anomalies over the North Atlantic (0 to 70N) which is then detrended. | NOAA AMO (or AMV) from ERSSTV5 | 1902-2024 | 1951-1980 | Enfield et al., (2001) |

| | | | | | | |
|---|---|---|---|---|---|---|
| IOD | Indian Ocean Dipole | Gradient of SST anomalies between the western equatorial Indian Ocean (50E-70E and 10S-10N) and the southeastern equatorial Indian Ocean (90E-110E and 10S-0N). | NOAA IOD (or DMI) from HadISST1.1 | 1902-2024 | 1981-2010 | Saji et al., (2003) |
| TPI | Tripole Index (Interdecadal Pacific Oscillation) | Difference between the SST anomalies of the central equatorial Pacific (170°E–90°W, 10°S–10°N) and the average of the northwest Pacific (140°E–145°W, 25°N–45°N) and southwest Pacific (150°E–160°W, 50°S–15°S). | NOAA TPI (or IPO) from HadISST1.1 | 1902-2024 | 1971-2000 | Henley et al. (2015) |
| AO | Arctic Oscillation | EOF of monthly mean of 1000-hPa HGT anomalies poleward of 20°N. | NOAA AO from NCEP/NCAR Reanalysis HGT | 1950-2024 | 1979-2000 | Thompson & Wallace (1998, 2000) |
| AAO | Antarctic Oscillation | EOF of monthly mean of 700-hPa HGT anomalies poleward of 20°S. | NOAA AAO from NCEP/NCAR Reanalysis HGT | 1979-2024 | 1979-2000 | Mo., (2000) |
| SAM | Southern Annular Mode | Standardized difference in zonal mean of sea level pressure between 40°S and 65°S | SAM from NOAA-CIRES-DOE Twentieth Century Reanalysis (20CR) | 1940-2011 | 1981-2010 | Gong & Wang, (1999) |
| NAO | North Atlantic Oscillation | EOF of SLP anomalies over the Atlantic sector (20°-80°N, 90°W-40°E) | NAO PC-Based from NCEP/NCAR SLP | 1948-2024 | 1948-2024 | Hurell., (1995) |
| NPI | North Pacific Index | Standardized area-weighted sea level pressure over the North Pacific region (30°N-65°N, 160°E-140°W) | NPI PC-Based from NCEP/NCAR SLP | 1948-2024 | - | Trenberth & Hurell., (1994) |

217

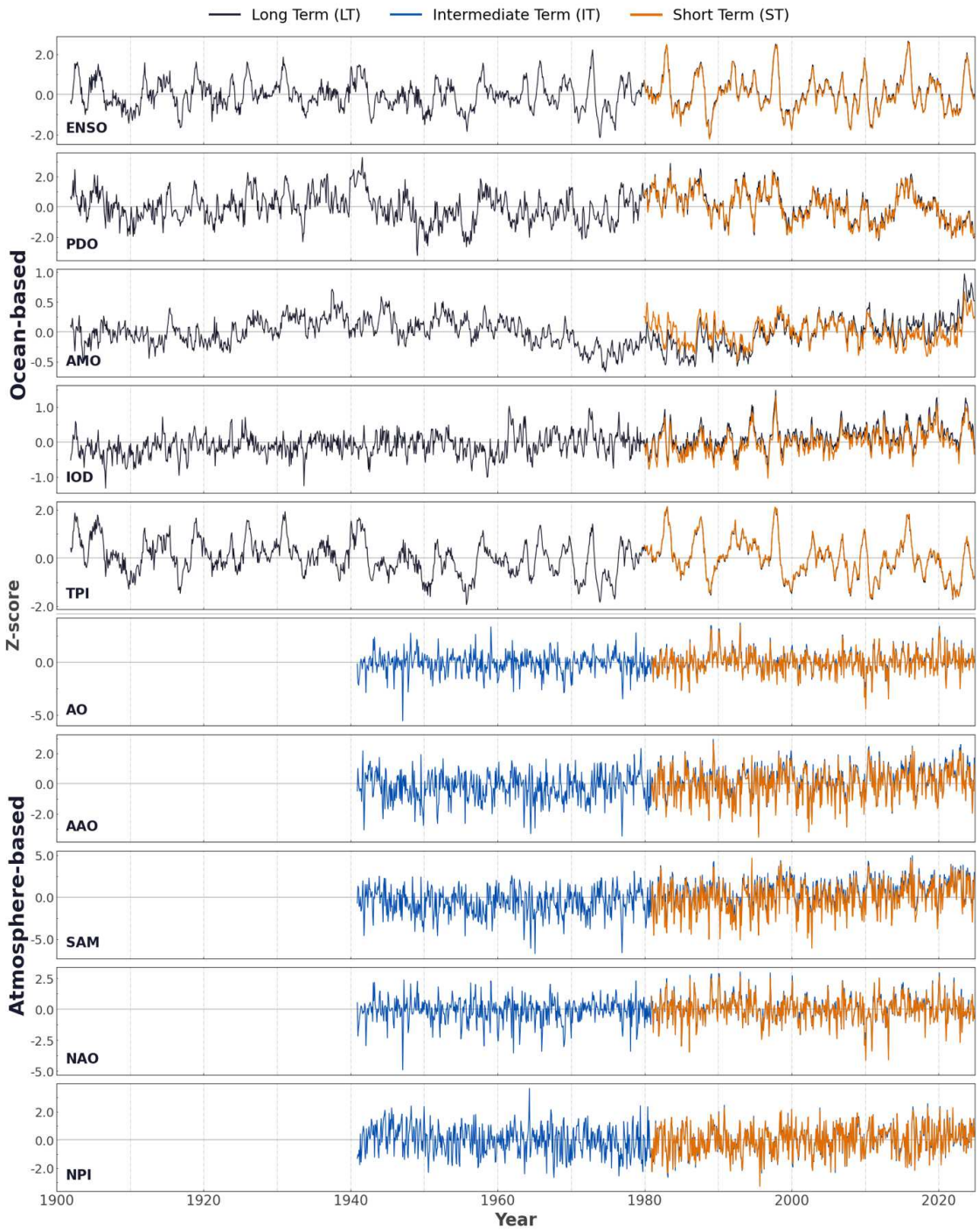



***Figure 2.*** *Systematized time series of ten large-scale climate indices across multiple temporal scales from the early 20th century to present. Ocean-based indices (ENSO, PDV, AMV, IOD, TPI) are computed over the long Term interval (1902-2024), while atmosphere-based indices (AO, AAO, SAM, NAO, NPI) cover an intermediate-term interval (1941–2024). All indices are also computed over the common Short-Term interval (1981-2024).*

### c. Hydroclimate Teleconnection Maps using Linear Regression

We calculate the grid point regression coefficients (expressed in units of anomalies of the hydroclimate variable per standard deviation of the index) and the Pearson correlation coefficients between each climate index and hydroclimate field (and SST field if applicable) during each season. Statistical significance for the regression and correlation coefficients is assessed using a two-tailed t-test at the 95% confidence level ($p < 0.025$).

The regressions and correlations were computed separately for each period: the LT period (1902-2024) for SST-based indices against CRU hydroclimate variables; the IT period (1941-2024) for HGT/SLP-based indices against CRU hydroclimate variables; and the ST period (1981-2024) with the latter available for all ten indices against CRU, GLEAM, and GPCP hydroclimate variables. We provide an example of the resulting maps (all of which are provided at the data product website at HYDRA) in Figures 3 and 4, which present the results for the ENSO index over the LT and ST periods.

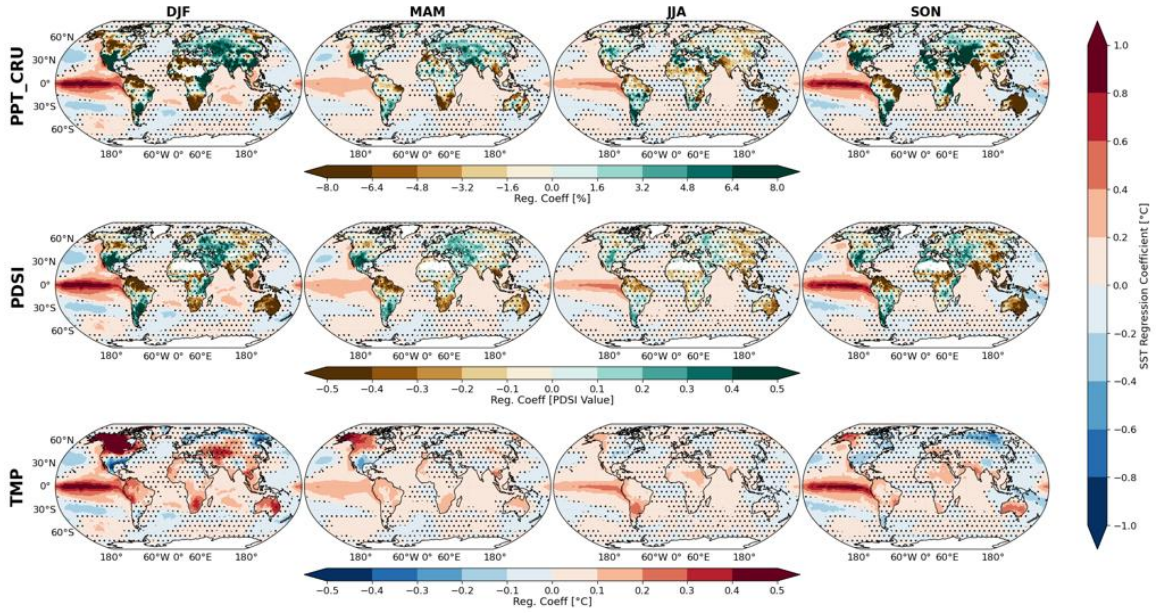



***Figure 3.*** *Teleconnection maps showing ENSO-related seasonal regression coefficients of PPT_CRU, PDSI, and TMP (temperature, bottom) onto the standardized NINO3.4 index for the long-term period (1902–2024); see variable definitions in Table 2. Stippling indicates statistically insignificant regions (p >0.05).*

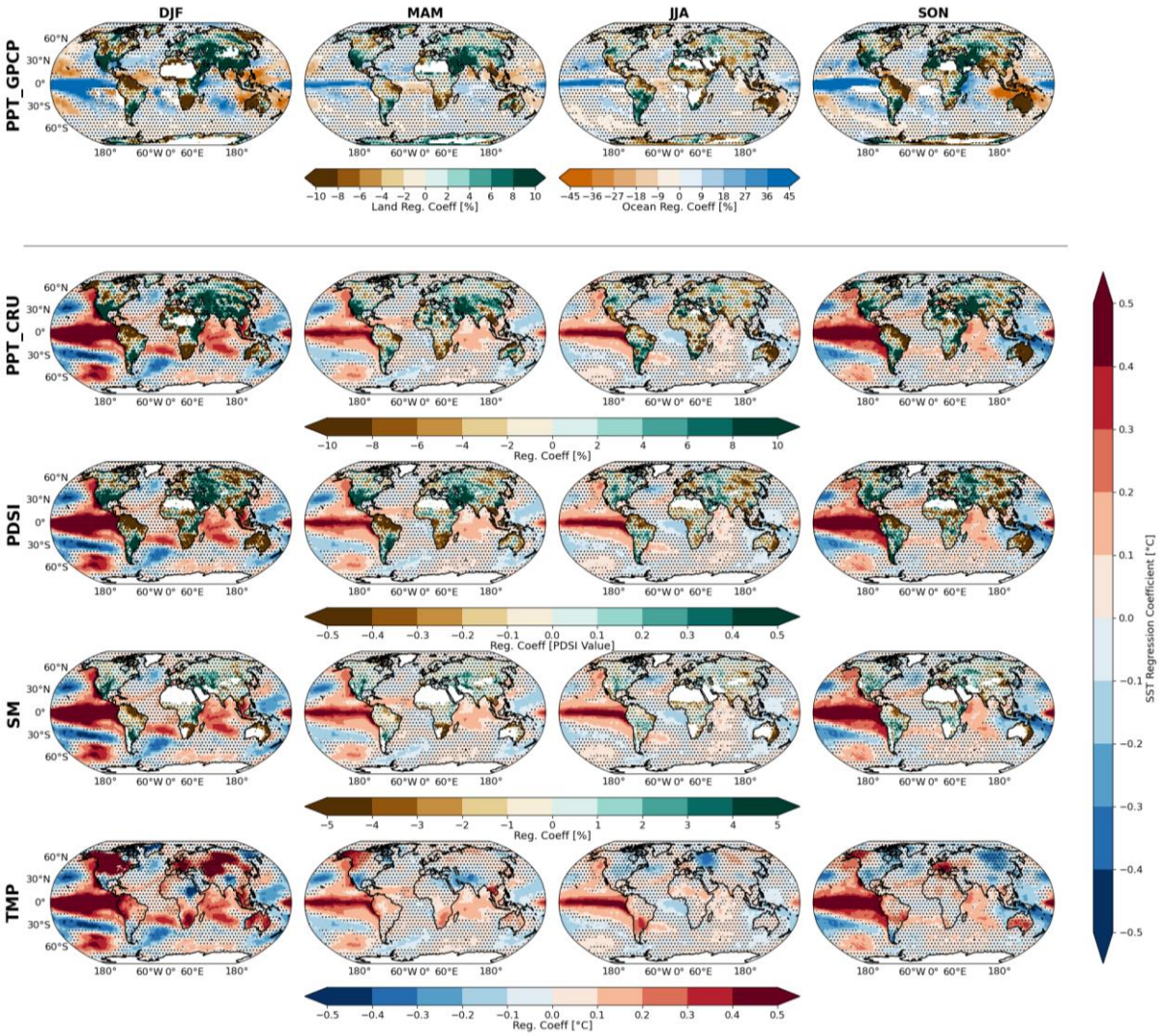



***Figure 4.*** *Teleconnection maps showing seasonal regression coefficients for PPT_GPCP, PPT_CRU, PDSI and TMP (temperature, bottom) regressed onto the ENSO index for the short-term period (1981–2024); see variable definitions in Table 2. Stippling indicates statistically insignificant regions (p > 0.05).*

### d. Identification of Extreme State of Climate Indices

For each of the ten climate indices and seasons, years were ranked by index magnitude for the upper and lower 15th percentiles to identify the years with extreme positive and negative phases, respectively. These extreme years are marked in Figure 5 for all indices over the ST interval.

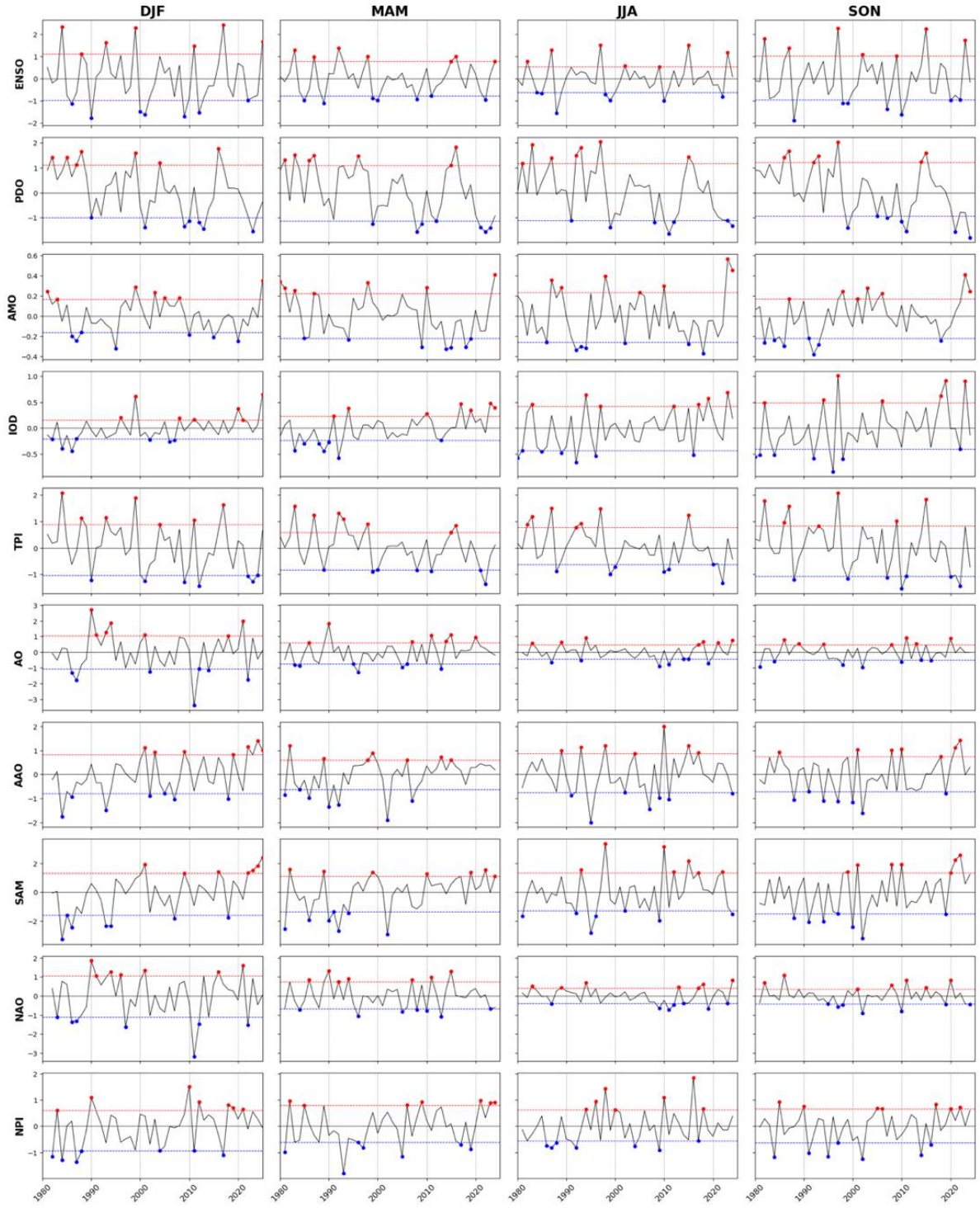



***Figure 5.*** *Seasonal time series of all climate indices over the short term (1981-2024) interval. For each index and season, years exceeding the upper and lower 15th percentile thresholds (dashed lines) are marked in red and blue dots, respectively. DJF years are assigned to the January–February calendar year.*

### e. Agreement Composites analysis

To characterize the spatial covariability between the large-scale climate indices and regional hydroclimate anomalies, we developed an agreement composite framework based on the overlap between extreme years of the climate index and extreme years of hydroclimate states. Unlike a regression or correlation coefficient that summarizes an average linear relationship, this framework identifies where an index's extreme-phase years align with hydroclimate extremes.
For each of the ten climate indices, we selected the years ranked in the upper and lower 15th percentiles, as described in the previous section. The corresponding hydroclimate field was ranked in time at each grid cell, and the upper and lower 15th percentiles of that field were selected. We then computed the agreement count as the number of years of overlap between the index's extreme-phase years and the grid cell's extreme hydroclimate years. The evaluation was done separately for all four phase combinations (index-positive/hydroclimate field-high, index-positive/ hydroclimate field-low, index-negative/ hydroclimate field-high, index-negative/ hydroclimate field-low). Spatial maps of overlap count for each index–hydroclimate field pair were derived from these comparisons. Areas with high agreement showcase where the most hydroclimate extremes robustly align with the index's extreme phase years. Examples of the results are shown for the Top $15^{th}$ Percentile for ENSO over the ST interval in Figure 6.

To account for the possibility that agreement counts may arise by chance, we estimated random-chance thresholds using a hypergeometric distribution parameterized by the total number of years (N) and the sample sizes of the years in the top and bottom 15th percentile. This was used to define fixed thresholds for categorizing agreement strength (none, low, medium, high), such that the color bar in Figure 6 corresponds to increasing departures from chance-level overlap (Feller, 1957). This was done separately for LT, IT and ST. A table with all the numbers of years selected for each period for the indices and the hydroclimate in those corresponding years is described in Table S1. Areas showing agreements above the defined thresholds were included while those below were masked out. Along with agreements, regions exhibiting conflicting signals were also excluded by masking. These are grid cells in which, for a given index phase, both the top and bottom 15th percentile of the hydroclimate field are represented among the composite years. This is to exclude regions that do not produce a coherent directional hydroclimate response for the extreme index years.

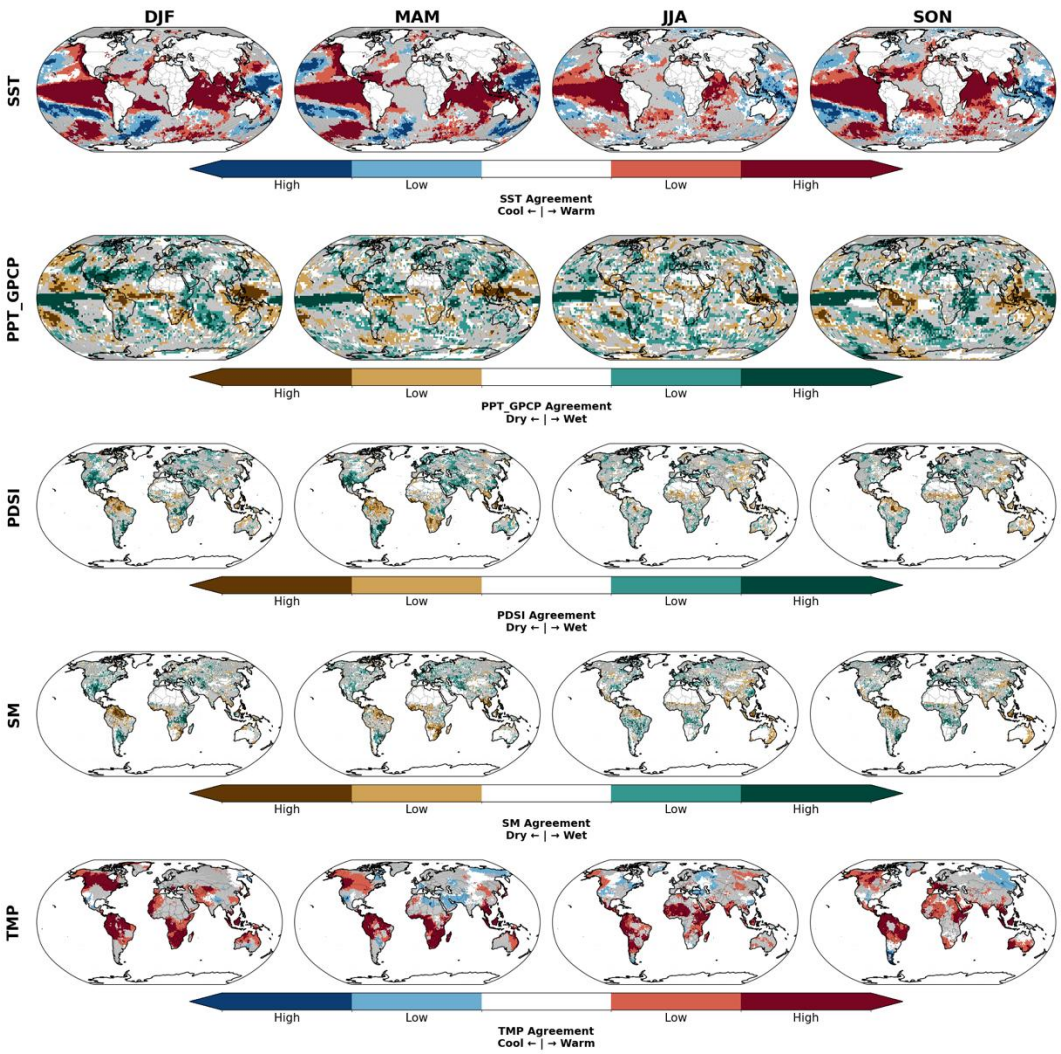



***Figure 6.*** *Agreement composite maps for SST and each of the hydroclimate fields (PPT_GPCP, PDSI, SM and TMP) for Top 15th Percentile of ENSO Years (El Niño states) over the short-term period (1981–2024) with agreement thresholds showing high and low agreement; see variable definitions in Table 2. Regions with agreement counts below the chance-level threshold are masked, while the grid cells showing ambiguous response (where both the top and bottom 15th percentiles of the hydroclimate field occur among a single index phase's composite years), are shown in grey.*

## 3. Data Records

All HYDRA products are freely available for exploration through the HYDRA website for download from zenodo, DOI 10.5281/zenodo.22956140, which has the time series, teleconnection maps, and agreement composites by index, season, variable, and for each of the analysis periods. A user interested in, for example, winter (DJF) teleconnection associated with El Niño could find

the seasonal PDSI regression map for the positive phase of ENSO over the 1981–2024 period directly from the site.

All datasets are provided as gridded fields and stored in NetCDF-4 format. Each file contains coordinate variables for latitude, longitude, and time, along with associated variable metadata including units, long name attributes, and missing values flagged as NaNs. The extreme states are additionally provided in comma-separated value (CSV) format. {

For all files, {PERIOD} references to the following:

- LT: long term (1902–2024), Only SST-based indices
- IT: intermediate term (1941–2024), Only HGT/SLP-based indices
- ST: short term (1981–2024), all indices

For all files, {VARIABLE} references to the following:

- For LT and IT: PDSI, PPT_CRU, TMP, SST
- For ST: PDSI, SM, PPT_CRU, PPT_GPCP, TMP, SST

**/indices/**: Computed climate index time series (monthly and seasonal, all periods):

- SST_INDEX_{PERIOD}
- ATM_INDEX_{PERIOD}

**/indices/val/**: Computed climate index time series used for comparison with online published reference indices for validation.

**/indices/ext_years/**: Contains the extreme-year tables, {INDEX}_EXT_YEARS_{PERIOD}.csv, which list the top and bottom 15% index years for each season (DJF, MAM, JJA, SON), ranked by magnitude, with their index values. DJF years are labelled by the January year.

**/teleconnections_{PERIOD}/**: Seasonal teleconnection maps of hydroclimate fields onto each climate index. There is one file per variable and period, named {VARIABLE}_REG_{PERIOD}.nc. Each file contains, for every index in that period, the regression coefficient and correlation p-value ({INDEX}_{VARIABLE}_reg, {INDEX}_{VARIABLE}_pvals) on a (season, lat, lon) grid at the variable's native resolution: 0.5° for PDSI, 2.5° for PPT_GPCP and 1° for all others.

**/agreements/**: Seasonal agreement composites showing how consistently each hydroclimate field reaches its own extremes during extreme index years. They are named {INDEX}_{VARIABLE}_AGR_{PHASE}_{PERIOD}.nc, where PHASE is TOP (top 15% of index years) or BOT (bottom 15%).

Each file contains two variables on a (season, lat, lon) grid:

- **{INDEX}_{VAR}_agr:** the signed count of index years in which the field was in its own top 15% (+n) or bottom 15% (−n). 0 means no extremes, and NaN marks overlap points.
- **{INDEX}_{VAR}_overlap**: 1 where both top and bottom extremes co-occurred during the selected years.

The global attributes record the index, variable, phase, period, percentile (15%), the maximum number of years per phase, and the selected index years for each season. All NetCDF files carry the HYDRA metadata and follow CF-1.8 and ACDD-1.3 conventions.

## 4. Technical Validation

### a. Index validation

Computed climate indices were validated by comparing each index time series against independently published and publicly available index products (Figure 7). All reference indices, and their sources, used for validation are listed in Table 1. To ensure methodological consistency, the same input datasets and the same climatological base period as the reference indices were used to compute the reconstructed indices for validation. Pearson correlation coefficients were computed for the reconstructed indices and reference indices, over the time period of the reference indices, all of which exceed $r = 0.98$ ($p < 0.05$) for all ten indices, validating that the methods for computation correctly reproduce the indices published online. Minor differences between the reconstructed indices for validation and reference products reflect differences in the re-gridding methods, differences in the version of the same dataset, and differences in the packages used for computing EOFs, rather than errors in the index methodology. Following successful validation, we use the systematized indices, and selected common LT, IT and ST time intervals, for all regression, correlation, extreme states and agreement composites in HYDRA.

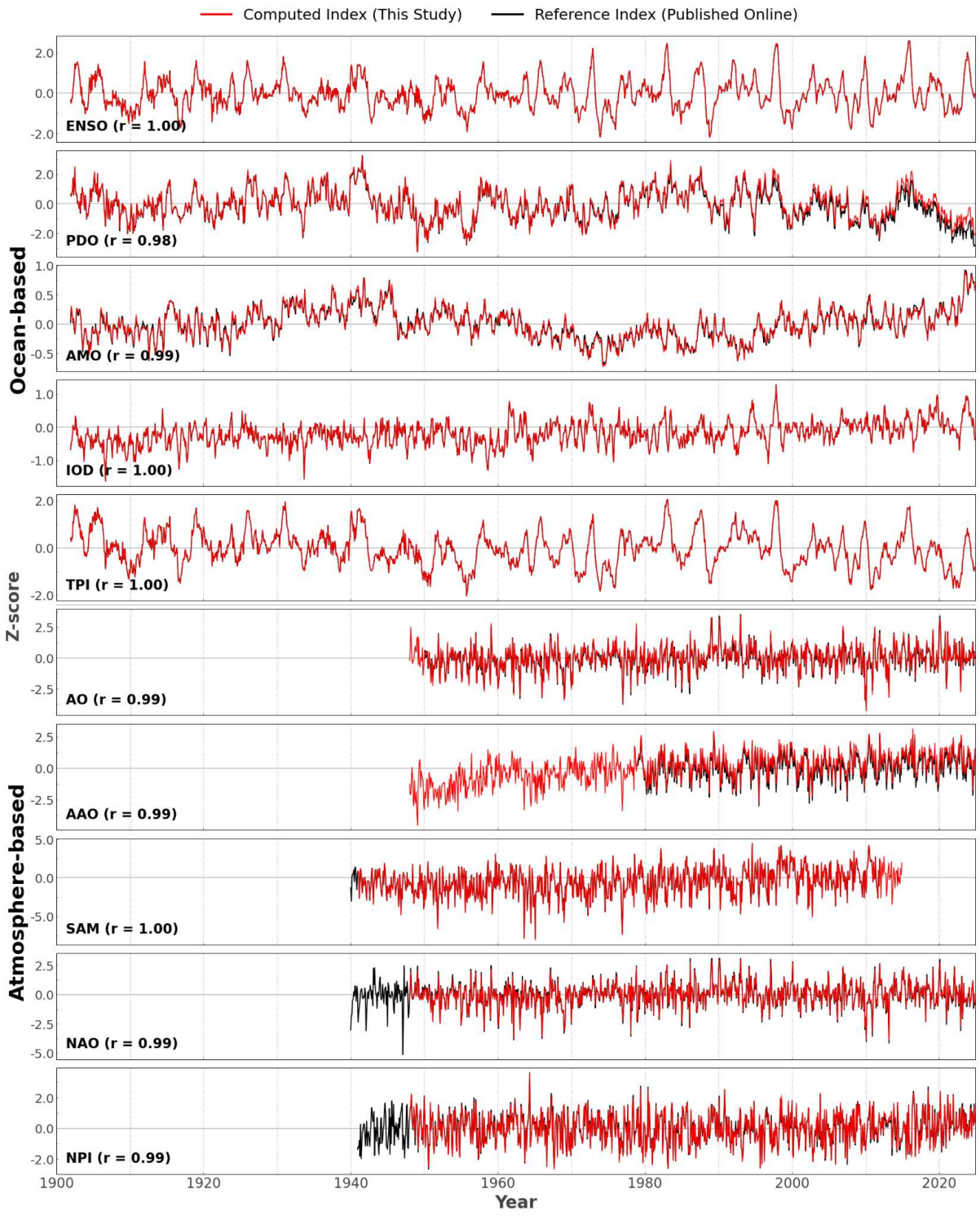



***Figure 7.*** *Validation of reconstructed climate index time series against reference datasets for ten large-scale climate modes. Pearson correlation coefficients between the validation and reference series are shown in each panel title.*

## 5. Usage Notes

### a. Research Use

**Example use case: Comparison of global hydroclimate impacts of ocean variability across seasons and the sources of SST-forced seasonal variability over North America**

In this section we provide an example of how HYDRA can be used in practice. A researcher interested in, say, hydroclimate variability over North America and how it depends on climate modes across seasons will typically find the literature fragmented, with separate analyses for winter and summer, each focused on the influence of a different ocean basin and often relying on different datasets, time periods, and methodologies. This leaves open questions such as: (1) whether the dominant driver of variability switches from one basin to another across the seasonal cycle; (2) whether the teleconnections from a given basin change in strength or pattern by season; and (3) how the impacts over North America fit into global ocean-atmosphere patterns? HYDRA aims to remove the ambiguity in the answers to these questions by providing a single, internally consistent atlas of hydroclimate variability, giving researchers the consistency, comprehensiveness, and inter-comparability these questions require.

The researcher will be aware that prior literature on North American hydroclimate variability has appealed to both Pacific and Atlantic forcing (e.g. Schubert et al. 2009) and, therefore, might first want to examine the patterns of how different climate modes impact PDSI and how this varies by season. Figure 8 provides teleconnection maps associated with the four SST-based indices, showing the associations with SST over the ocean and PDSI over land and across the four seasons for the LT. During its El Niño phase, ENSO produces a clear north–south dipole over the continent with a pronounced wetting across the southern region, paired with drying farther north. This pattern peaks in DJF and is weakest in JJA, which is consistent with ENSO's North American teleconnection acting mainly through the winter storm track and jet stream position (A. Kumar & Hoerling, 1998; Mason & Goddard, 2001; Seager et al., 2005; Trenberth, 1997). The PDO shows a similar dipole but with substantially greater reach, its northern drying signal extending much farther poleward than ENSO's, reaching the eastern and northern Alaskan coast. This could be related to the greater North Pacific expression of the PDO relative to ENSO. The PDO also retains expression over North America in summer. While its summer tropical Pacific SST expression is also stronger than ENSO, this still requires dynamical explanation and could again be related to its strength in the North Pacific. The IOD and AMO, by comparison, leave more muted imprints on North American hydroclimate. IOD's clearest signal emerges in SON, during which the index itself is the most active, by bringing wetting to central North America and Alaska. AMO's strongest influence also falls in SON, wetting Alaska while drying the rest of the continent. This drying footprint then reduces to a region constrained to Canada in JJA and only over the Southwest in DJF.

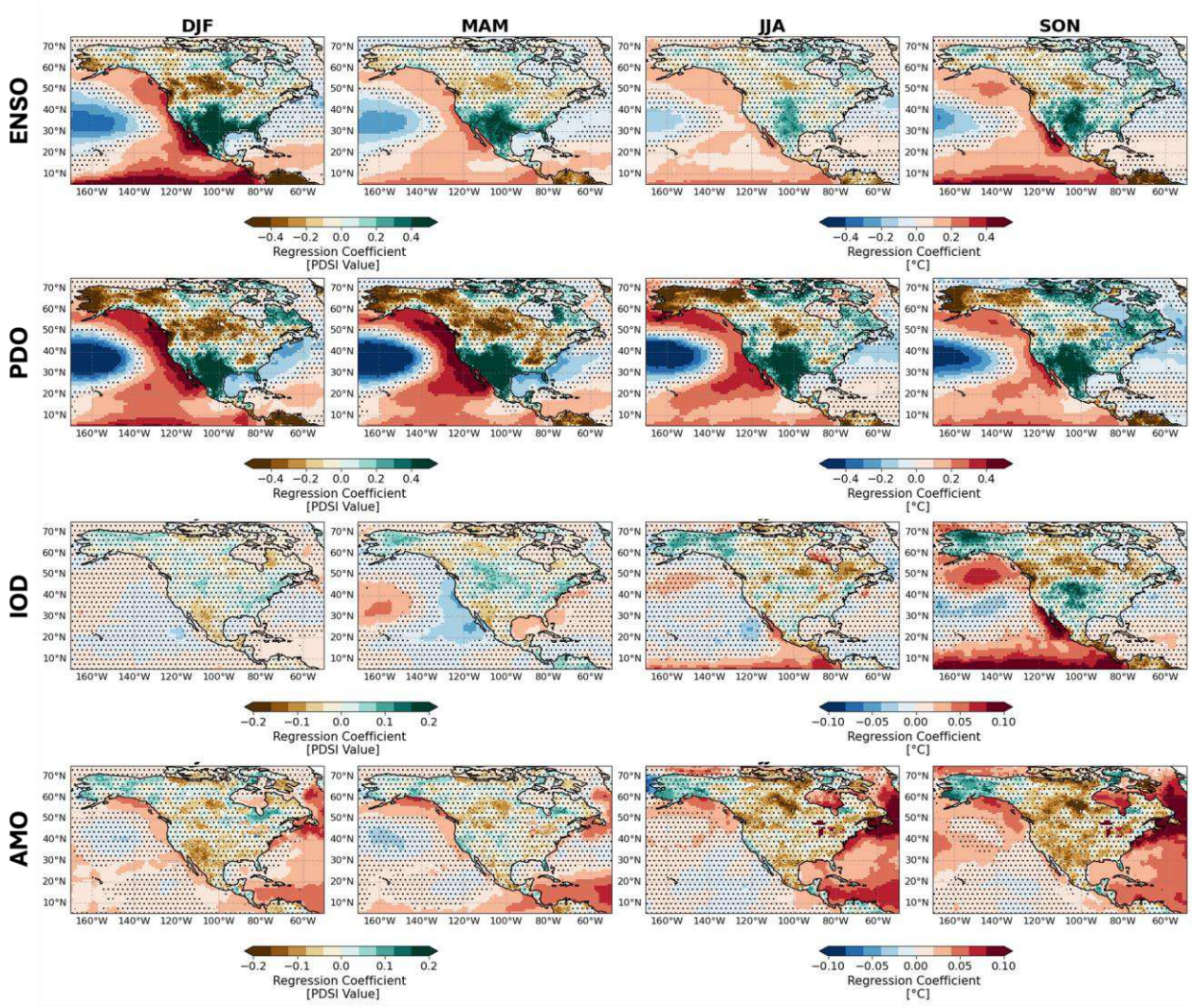



***Figure 8.*** *Teleconnection maps showing seasonal maps of PDSI (land) and SST (ocean) regressed onto the ENSO, PDO, IOD, and AMO indices over North America for the long-term period (1902–2024). Stippling indicates statistically insignificant regions (p > 0.05).*

Moving beyond North America and focusing on just ENSO and AMO, Figure 9 indicates how the ocean basin influences on North America, and their variation across seasons, fits into global hydroclimate variability. In addition to its influence on North America, ENSO's signal in its El Niño phase, strongest in SON and DJF, drives pronounced drying over northern South America, South Asia, and the Indo-Australian region, alongside wetting over southern South America, East Africa, and the Middle East into Central Asia; the same spatial pattern persists through MAM and JJA but weakens considerably. AMO, by contrast, exerts an influence of comparable magnitude across all four seasons, peaking modestly in JJA, with a distinct fingerprint of wetting over the Sahel and India and drying across South America (Enfield et al., 2001b; Knight et al., 2006; Ting

et al., 2011; R. Zhang et al., 2019; R. Zhang & Delworth, 2006). The two indices have clear differences in the regional pattern, strength, and seasonality of their influence.

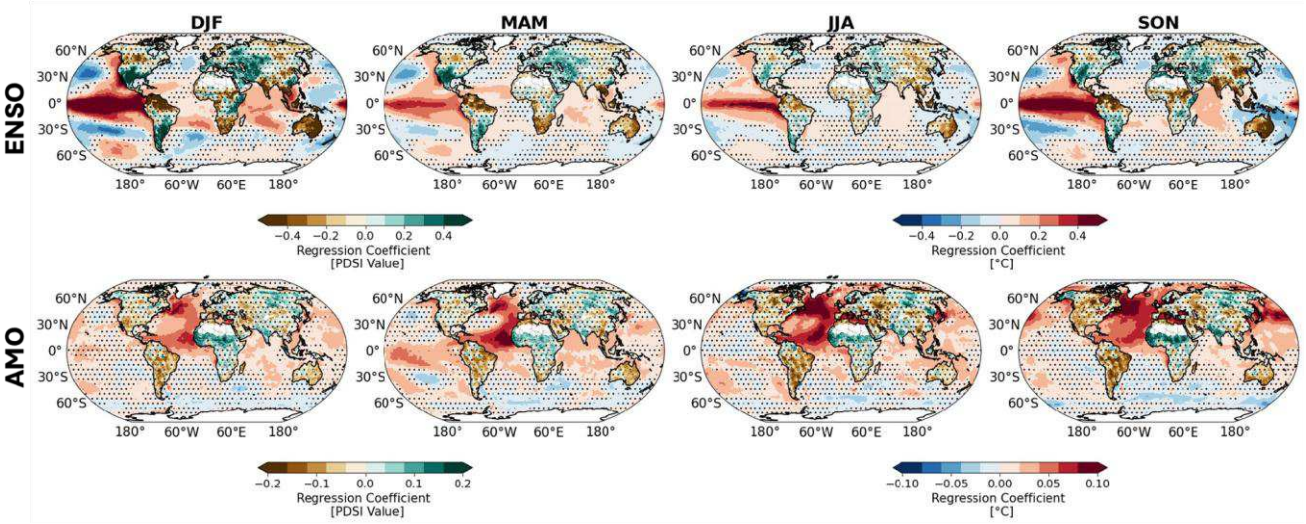



***Figure 9.*** *Teleconnection maps showing seasonal regression coefficients for PDSI and SST regressed onto the ENSO and AMO index for the long-term period (1902–2024). Stippling indicates statistically insignificant regions ($p > 0.05$).*

This HYDRA-based analysis helps answer the three original research questions posed in this example. Over North America, ENSO and PDO govern the winter half of the year, producing the strongest and most coherent wetting/drying dipole over North America in DJF, while IOD and AMO become more important in SON, the season in which their variability is strongest (Neelin et al., 2000; Stein et al., 2014). These results are indicative of the fact that there is a change in which basin is the dominant driver governing North American hydroclimate across the seasonal cycle. While each index retains a broadly consistent spatial signature across seasons, ENSO's north–south dipole and AMO's Alaska-wetting/continent-drying pattern, their strength varies considerably, peaking in DJF for ENSO/PDO and SON for IOD/AMO, and exerting strong influence over smaller regions in other seasons as found in previous literature (Neelin et al., 2000; Stein et al., 2014). Furthermore, the impacts over North America fit into coherent global patterns. The ocean basin-based modes that structure North American moisture anomalies leave comparable, and in some cases stronger, fingerprints elsewhere. From ENSO's drying over northern South America and South Asia to AMO's wetting over the Sahel and India, the North American regional response is just one expression of coherent, global ocean–atmosphere teleconnections that represent temporal planet-wide rearrangements of the climate system.

None of the above findings individually are novel. What is novel, however, is their integration and that they were derived based on common data sets, time periods, and verified definitions of modes. As such, they immediately answer the posed questions concerning which oceans and

modes exert control on North American hydroclimate, how that varies by season, and how it fits into global patterns of climate anomalies.

### b. Technical Usage:

A conda environment file (hydra_env.yml) is provided in the repository to help installation of the python package dependencies. The interactive web platform, Hydrological Drought and Rainfall Atlas (available at HYDRA), provides a visual interface for exploring all the teleconnection patterns in terms of regression and agreement composites. All CRU-based analyses are restricted to available land grid points with the ocean grid points masked. When working across periods, note that SST-based indices (ENSO_Index, PDO_Index, AMO_Index, IOD_Index, TPI_Index) and HGT and SLP-based indices (NAO_Index, PNA_Index, AO_Index, AAO_Index, SAM_Index) do not share the same baseline for the longer time comparison. For SST-indices, the baseline is from 1902-2024, while for the HGT and SLP-based indices, it is from 1941-2024. When interpreting maps, it also should be noted that these indices are not fully independent. For example, the ENSO, PDO, and TPI indices share Pacific SST variance through their physical coupling. Regarding the SAM and AAO, note they are often used interchangeably, but in keeping with literature definitions, we compute SAM from SLP and AAO from HGT (as defined in Table 1).

## 6. Data Availability

All gridded teleconnection maps of regressions and agreement composite datasets described in this paper are freely available at Zenodo, DOI: 10.5281/zenodo.22956140. Climate index time series are available in both NetCDF-4 and CSV formats at the same repository. The interactive web platform is available at HYDRA. Input datasets used in this atlas are available from their respective providers: HadISST (www.metoffice.gov.uk/hadobs/hadisst), CRU TS v4.08 (crudata.uea.ac.uk/cru/data/hrg), ERA5 (cds.climate.copernicus.eu), GLEAM v4.02 (www.gleam.eu), and GPCP v2.3 (https://psl.noaa.gov/data/gridded/data.gpcp.html).

## 7. Code Availability

All Python code used to compute climate indices, perform regression and agreement composite analyses, and generate figures is available at GitHub link under /notebooks.

## 8. Author Contributions

A.T.S. conceived the study, performed the analysis, and wrote the manuscript. J.E.S. and R.S. provided overall guidance, developed the analyses with A.S., and edited the manuscript.

## 9. Competing Interests

The authors declare no competing interests.

## 10. Acknowledgements

Support for the Twentieth Century Reanalysis Project version 2c dataset is provided by the U.S. Department of Energy, Office of Science Biological and Environmental Research (BER), and by the National Oceanic and Atmospheric Administration Climate Program Office.

## 11. Funding:

This work was supported by the National Science Foundation under Grants AGS-2127684 and AGS-2101214.

## 12. Reference:


Adler, R. F., Huffman, G. J., Chang, A., Ferraro, R., Xie, P.-P., Janowiak, J., Rudolf, B., Schneider, U., Curtis, S., Bolvin, D., Gruber, A., Susskind, J., Arkin, P., & Nelkin, E. (2003). *The Version-2 Global Precipitation Climatology Project (GPCP) Monthly Precipitation Analysis (1979–Present)*. https://journals.ametsoc.org/view/journals/hydr/4/6/1525-7541_2003_004_1147_tvgpcp_2_0_co_2.xml

AghaKouchak, A., Mirchi, A., Madani, K., Di Baldassarre, G., Nazemi, A., Alborzi, A., Anjileli, H., Azarderakhsh, M., Chiang, F., Hassanzadeh, E., Huning, L. S., Mallakpour, I., Martinez, A., Mazdiyasni, O., Moftakhari, H., Norouzi, H., Sadegh, M., Sadeqi, D., Van Loon, A. F., & Wanders, N. (2021). Anthropogenic Drought: Definition, Challenges, and Opportunities. *Reviews of Geophysics*, *59*(2), e2019RG000683. https://doi.org/10.1029/2019RG000683

Alizadeh, O. (2024). A review of ENSO teleconnections at present and under future global warming. *WIREs Climate Change*, *15*(1), e861. https://doi.org/10.1002/wcc.861

Allan, R. P., & Soden, B. J. (2008). Atmospheric Warming and the Amplification of Precipitation Extremes. *Science*, *321*(5895), 1481–1484. https://doi.org/10.1126/science.1160787

Andreoli, R. V., & Kayano, M. T. (2005). ENSO-related rainfall anomalies in South America and associated circulation features during warm and cold Pacific decadal oscillation regimes. *International Journal of Climatology*, *25*(15), 2017–2030. https://doi.org/10.1002/joc.1222

Ashok, K., Guan, Z., & Yamagata, T. (2001). Impact of the Indian Ocean dipole on the relationship between the Indian monsoon rainfall and ENSO. *Geophysical Research Letters*, *28*(23), 4499–4502. https://doi.org/10.1029/2001GL013294

Ashok, K., & Saji, N. H. (2007). On the impacts of ENSO and Indian Ocean dipole events on sub-regional Indian summer monsoon rainfall. *Natural Hazards*, *42*(2), 273–285. https://doi.org/10.1007/s11069-006-9091-0

Barnston, A. G., & Livezey, R. E. (1987). *Classification, Seasonality and Persistence of Low-Frequency Atmospheric Circulation Patterns*. https://journals.ametsoc.org/view/journals/mwre/115/6/1520-0493_1987_115_1083_csapol_2_0_co_2.xml

Bell, B., Hersbach, H., Simmons, A., Berrisford, P., Dahlgren, P., Horányi, A., Muñoz-Sabater, J., Nicolas, J., Radu, R., Schepers, D., Soci, C., Villaume, S., Bidlot, J.-R., Haimberger, L., Woollen, J., Buontempo, C., & Thépaut, J.-N. (2021). The ERA5 global reanalysis:

Preliminary extension to 1950. *Quarterly Journal of the Royal Meteorological Society*, *147*(741), 4186–4227. https://doi.org/10.1002/qj.4174

Biasutti, M. (2019). Rainfall trends in the African Sahel: Characteristics, processes, and causes. *WIREs Climate Change*, *10*(4), e591. https://doi.org/10.1002/wcc.591

Buckley, M. W., & Marshall, J. (2016). Observations, inferences, and mechanisms of the Atlantic Meridional Overturning Circulation: A review. *Reviews of Geophysics*, *54*(1), 5–63. https://doi.org/10.1002/2015RG000493

Cai, W., McPhaden, M. J., Grimm, A. M., Rodrigues, R. R., Taschetto, A. S., Garreaud, R. D., Dewitte, B., Poveda, G., Ham, Y.-G., Santoso, A., Ng, B., Anderson, W., Wang, G., Geng, T., Jo, H.-S., Marengo, J. A., Alves, L. M., Osman, M., Li, S., … Vera, C. (2020). Climate impacts of the El Niño–Southern Oscillation on South America. *Nature Reviews Earth & Environment*, *1*(4), 215–231. https://doi.org/10.1038/s43017-020-0040-3

Capotondi, A., Deser, C., Phillips, A. S., Okumura, Y., & Larson, S. M. (2020). ENSO and Pacific Decadal Variability in the Community Earth System Model Version 2. *Journal of Advances in Modeling Earth Systems*, *12*(12), e2019MS002022. https://doi.org/10.1029/2019MS002022

Capotondi, A., Wittenberg, A. T., Newman, M., Lorenzo, E. D., Yu, J.-Y., Braconnot, P., Cole, J., Dewitte, B., Giese, B., Guilyardi, E., Jin, F.-F., Karnauskas, K., Kirtman, B., Lee, T., Schneider, N., Xue, Y., & Yeh, S.-W. (2015). *Understanding ENSO Diversity*. https://doi.org/10.1175/BAMS-D-13-00117.1

Cayan, D. R., Redmond, K. T., & Riddle, L. G. (1999). *ENSO and Hydrologic Extremes in the Western United States*. https://journals.ametsoc.org/view/journals/clim/12/9/1520-0442_1999_012_2881_eaheit_2.0.co_2.xml

Chan, D., Kent, E. C., Lenssen, N., Deser, C., Merchant, C. J., Ishii, M., Sandford, C., Huang, B., Yin, X., Kennedy, J. J., Cornes, R. C., Huybers, P., & Gebbie, G. (2026). Choosing the Right Sea Surface Temperature Datasets: Benchmarking and Guidance for Climate Applications. *Bulletin of the American Meteorological Society*, *1*(aop). https://doi.org/10.1175/BAMS-D-25-0210.1

Chen, X., & Wallace, J. M. (2015). ENSO-Like Variability: 1900–2013*. *Journal of Climate*, *28*(24), 9623–9641. https://doi.org/10.1175/JCLI-D-15-0322.1

Chen, Z., Wu, R., Zhao, Y., & Wang, Z. (2022). *Different Responses of Central Asian Precipitation to Strong and Weak El Niño Events*. https://doi.org/10.1175/JCLI-D-21-0238.1

Cheung, A. H., Smerdon, J. E., Li, C., & Steiger, N. J. (2025). *Proxy- and Model-Estimated Coupled Megadroughts in the Southwestern Regions of North and South America*. https://doi.org/10.1175/JCLI-D-24-0383.1

Chiang, J. C. H., & Sobel, A. H. (2002). *Tropical Tropospheric Temperature Variations Caused by ENSO and Their Influence on the Remote Tropical Climate*. https://journals.ametsoc.org/view/journals/clim/15/18/1520-0442_2002_015_2616_tttvcb_2.0.co_2.xml

Chiew, F. H. S., Piechota, T. C., Dracup, J. A., & McMahon, T. A. (1998). El Nino/Southern Oscillation and Australian rainfall, streamflow and drought: Links and potential for forecasting. *Journal of Hydrology*, *204*(1), 138–149. https://doi.org/10.1016/S0022-1694(97)00121-2

Cole, J. E., Overpeck, J. T., & Cook, E. R. (2002). Multiyear La Niña events and persistent drought in the contiguous United States. *Geophysical Research Letters*, *29*(13), 25-1-25–4. https://doi.org/10.1029/2001GL013561

Cronin, M. F., Gentemann, C. L., Edson, J., Ueki, I., Bourassa, M., Brown, S., Clayson, C. A., Fairall, C. W., Farrar, J. T., Gille, S. T., Gulev, S., Josey, S. A., Kato, S., Katsumata, M., Kent, E., Krug, M., Minnett, P. J., Parfitt, R., Pinker, R. T., … Zhang, D. (2019). Air-Sea Fluxes With a Focus on Heat and Momentum. *Frontiers in Marine Science*, *6*. https://doi.org/10.3389/fmars.2019.00430

Dai, A., & Wigley, T. M. L. (2000). Global patterns of ENSO-induced precipitation. *Geophysical Research Letters*, *27*(9), 1283–1286. https://doi.org/10.1029/1999GL011140

Deser, C., Alexander, M. A., Xie, S.-P., & Phillips, A. S. (2010). Sea Surface Temperature Variability: Patterns and Mechanisms. *Annual Review of Marine Science*, *2*(1), 115–143. https://doi.org/10.1146/annurev-marine-120408-151453

Deser, C., Lehner, F., Rodgers, K. B., Ault, T., Delworth, T. L., DiNezio, P. N., Fiore, A., Frankignoul, C., Fyfe, J. C., Horton, D. E., Kay, J. E., Knutti, R., Lovenduski, N. S., Marotzke, J., McKinnon, K. A., Minobe, S., Randerson, J., Screen, J. A., Simpson, I. R., & Ting, M. (2020). Insights from Earth system model initial-condition large ensembles and future prospects. *Nature Climate Change*, *10*(4), 277–286. https://doi.org/10.1038/s41558-020-0731-2

Deser, C., Simpson, I. R., McKinnon, K. A., & Phillips, A. S. (2017). *The Northern Hemisphere Extratropical Atmospheric Circulation Response to ENSO: How Well Do We Know It and How Do We Evaluate Models Accordingly?* https://doi.org/10.1175/JCLI-D-16-0844.1

Enfield, D. B., Mestas-Nuñez, A. M., & Trimble, P. J. (2001a). The Atlantic Multidecadal Oscillation and its relation to rainfall and river flows in the continental U.S. *Geophysical Research Letters*, *28*(10), 2077–2080. https://doi.org/10.1029/2000GL012745

Enfield, D. B., Mestas-Nuñez, A. M., & Trimble, P. J. (2001b). The Atlantic Multidecadal Oscillation and its relation to rainfall and river flows in the continental U.S. *Geophysical Research Letters*, *28*(10), 2077–2080. https://doi.org/10.1029/2000GL012745

Eyring, V., Righi, M., Lauer, A., Evaldsson, M., Wenzel, S., Jones, C., Anav, A., Andrews, O., Cionni, I., Davin, E. L., Deser, C., Ehbrecht, C., Friedlingstein, P., Gleckler, P., Gottschaldt, K.-D., Hagemann, S., Juckes, M., Kindermann, S., Krasting, J., … Williams, K. D. (2016). ESMValTool (v1.0) – a community diagnostic and performance metrics tool for routine evaluation of Earth system models in CMIP. *Geoscientific Model Development*, *9*(5), 1747–1802. https://doi.org/10.5194/gmd-9-1747-2016

Fasullo, J. T., Phillips, A. S., & Deser, C. (2020). *Evaluation of Leading Modes of Climate Variability in the CMIP Archives*. https://doi.org/10.1175/JCLI-D-19-1024.1

Fogt, R. L., & Marshall, G. J. (2020). The Southern Annular Mode: Variability, trends, and climate impacts across the Southern Hemisphere. *WIREs Climate Change*, *11*(4), e652. https://doi.org/10.1002/wcc.652

Foltz, G. R., Brandt, P., Richter, I., Rodríguez-Fonseca, B., Hernandez, F., Dengler, M., Rodrigues, R. R., Schmidt, J. O., Yu, L., Lefevre, N., Da Cunha, L. C., McPhaden, M. J., Araujo, M., Karstensen, J., Hahn, J., Martín-Rey, M., Patricola-DiRosario, C. M., Poli, P., Zuidema, P., … Reul, N. (2019). The Tropical Atlantic Observing System. *Frontiers in Marine Science*, *6*, 206. https://doi.org/10.3389/fmars.2019.00206

Giannini, A., Saravanan, R., & Chang, P. (2003). Oceanic forcing of Sahel rainfall on interannual to interdecadal time scales. *Science*, *302*(5647), 1027–1030. https://doi.org/10.1126/science.1089357

Gillett, N. P., Kell, T. D., & Jones, P. D. (2006). Regional climate impacts of the Southern Annular Mode. *Geophysical Research Letters*, *33*(23). https://doi.org/10.1029/2006GL027721

Gong, D., & Wang, S. (1999). Definition of Antarctic Oscillation index. *Geophysical Research Letters*, *26*(4), 459–462. https://doi.org/10.1029/1999GL900003

Grimm, A. M., Barros, V. R., & Doyle, M. E. (2000). Climate Variability in Southern South America Associated with El Niño and La Niña Events. *Journal of Climate*, *13*(1), 35–58. https://doi.org/10.1175/1520-0442(2000)013%3C0035:CVISSA%3E2.0.CO;2

Grimm, A. M., & Tedeschi, R. G. (2009). *ENSO and Extreme Rainfall Events in South America*. https://doi.org/10.1175/2008JCLI2429.1

Grise, K. M., Davis, S. M., Simpson, I. R., Waugh, D. W., Fu, Q., Allen, R. J., Rosenlof, K. H., Ummenhofer, C. C., Karnauskas, K. B., Maycock, A. C., Quan, X.-W., Birner, T., & Staten, P. W. (2019). Recent Tropical Expansion: Natural Variability or Forced Response? *Journal of Climate*, *32*(5), 1551–1571. https://doi.org/10.1175/JCLI-D-18-0444.1

Hanley, D. E., Bourassa, M. A., O'Brien, J. J., Smith, S. R., & Spade, E. R. (2003). *A Quantitative Evaluation of ENSO Indices*. https://journals.ametsoc.org/view/journals/clim/16/8/1520-0442_2003_16_1249_aqeoei_2.0.co_2.xml

Harris, I., Osborn, T. J., Jones, P., & Lister, D. (2020). Version 4 of the CRU TS monthly high-resolution gridded multivariate climate dataset. *Scientific Data*, *7*(1), 109. https://doi.org/10.1038/s41597-020-0453-3

He, C., Patrizio, C. R., Kwon, Y.-O., & Bellomo, K. (2026). North Atlantic Sea Surface Temperature Variability: Impacts, Mechanisms, and Challenges. *WIREs Climate Change*, *17*(3), e70077. https://doi.org/10.1002/wcc.70077

Henley, B. J., Gergis, J., Karoly, D. J., Power, S., Kennedy, J., & Folland, C. K. (2015). A Tripole Index for the Interdecadal Pacific Oscillation. *Climate Dynamics*, *45*(11), 3077–3090. https://doi.org/10.1007/s00382-015-2525-1

Hersbach, H., Bell, B., Berrisford, P., Hirahara, S., Horányi, A., Muñoz-Sabater, J., Nicolas, J., Peubey, C., Radu, R., Schepers, D., Simmons, A., Soci, C., Abdalla, S., Abellan, X., Balsamo, G., Bechtold, P., Biavati, G., Bidlot, J., Bonavita, M., … Thépaut, J.-N. (2020). The ERA5 global reanalysis. *Quarterly Journal of the Royal Meteorological Society*, *146*(730), 1999–2049. https://doi.org/10.1002/qj.3803

Hoerling, M., & Kumar, A. (2003). The Perfect Ocean for Drought. *Science*, *299*(5607), 691–694. https://doi.org/10.1126/science.1079053

Hurrell, J. W. (1995). Decadal Trends in the North Atlantic Oscillation: Regional Temperatures and Precipitation. *Science*, *269*(5224), 676–679. https://doi.org/10.1126/science.269.5224.676

Hurrell, J. W., Kushnir, Y., Ottersen, G., & Visbeck, M. (2003). An Overview of the North Atlantic Oscillation. In *The North Atlantic Oscillation: Climatic Significance and Environmental Impact* (pp. 1–35). American Geophysical Union (AGU). https://doi.org/10.1029/134GM01

IPCC. (2023). *AR6 Synthesis Report: Climate Change 2023*. https://www.ipcc.ch/report/ar6/syr/

Janicot, S., Trzaska, S., & Poccard, I. (2001). Summer Sahel-ENSO teleconnection and decadal time scale SST variations. *Climate Dynamics*, *18*(3), 303–320. https://doi.org/10.1007/s003820100172

Ju, J., & Slingo, J. (1995). The Asian summer monsoon and ENSO. *Quarterly Journal of the Royal Meteorological Society*, *121*(525), 1133–1168. https://doi.org/10.1002/qj.49712152509

Juneng, L., & Tangang, F. T. (2005). Evolution of ENSO-related rainfall anomalies in Southeast Asia region and its relationship with atmosphere–ocean variations in Indo-Pacific sector. *Climate Dynamics*, *25*(4), 337–350. https://doi.org/10.1007/s00382-005-0031-6

Knight, J. R., Folland, C. K., & Scaife, A. A. (2006). Climate impacts of the Atlantic Multidecadal Oscillation. *Geophysical Research Letters*, *33*(17). https://doi.org/10.1029/2006GL026242

Kumar, A., & Hoerling, M. P. (1998). Annual Cycle of Pacific–North American Seasonal Predictability Associated with Different Phases of ENSO. *Journal of Climate*, *11*(12), 3295–3308. https://doi.org/10.1175/1520-0442(1998)011%3C3295:ACOPNA%3E2.0.CO;2

Kumar, K. K., Rajagopalan, B., & Cane, M. A. (1999). On the Weakening Relationship Between the Indian Monsoon and ENSO. *Science*, *284*(5423), 2156–2159. https://doi.org/10.1126/science.284.5423.2156

Kumar, K. K., Rajagopalan, B., Hoerling, M., Bates, G., & Cane, M. (2006). Unraveling the Mystery of Indian Monsoon Failure During El Niño. *Science*, *314*(5796), 115–119. https://doi.org/10.1126/science.1131152

Kundzewicz, Z. W., Szwed, M., & Pińskwar, I. (2019). Climate Variability and Floods—A Global Review. *Water*, *11*(7), 1399. https://doi.org/10.3390/w11071399

Lehner, F., Deser, C., Simpson, I. R., & Terray, L. (2018). Attributing the U.S. Southwest's Recent Shift Into Drier Conditions. *Geophysical Research Letters*, *45*(12), 6251–6261. https://doi.org/10.1029/2018GL078312

L'Heureux, M. L., Tippett, M. K., Wheeler, M. C., Nguyen, H., Narsey, S., Johnson, N., Hu, Z.-Z., Watkins, A. B., Lucas, C., Ganter, C., Becker, E., Wang, W., & Di Liberto, T. (2024). A Relative Sea Surface Temperature Index for Classifying ENSO Events in a Changing Climate. *Journal of Climate*, *37*(4), 1197–1211. https://doi.org/10.1175/JCLI-D-23-0406.1

Li, J., Roughan, M., & Kerry, C. (2022). *Variability and Drivers of Ocean Temperature Extremes in a Warming Western Boundary Current*. https://doi.org/10.1175/JCLI-D-21-0622.1

Li, J., Wang, Z., Wu, X., Xu, C.-Y., Guo, S., Chen, X., & Zhang, Z. (2021). Robust Meteorological Drought Prediction Using Antecedent SST Fluctuations and Machine Learning. *Water Resources Research*, *57*(8), e2020WR029413. https://doi.org/10.1029/2020WR029413

Liu, J., Wu, D., Xu, X., Ji, M., Chen, Q., & Wang, X. (2021). Projection of extreme precipitation induced by Arctic amplification over the Northern Hemisphere. *Environmental Research Letters*, *16*(7), 074012. https://doi.org/10.1088/1748-9326/ac0acc

Ma, Y., Sun, J., Dong, T., Yu, W., & Dong, W. (2023). More profound impact of CP ENSO on Australian spring rainfall in recent decades. *Climate Dynamics*, *60*(9), 3065–3079. https://doi.org/10.1007/s00382-022-06485-w

Maher, N., Phillips, A. S., Deser, C., Wills, R. C. J., Lehner, F., Fasullo, J., Caron, J. M., Brunner, L., Beyerle, U., & Jeffree, J. (2025). The updated Multi-Model Large Ensemble Archive and the Climate Variability Diagnostics Package: New tools for the study of climate variability and change. *Geoscientific Model Development*, *18*(18), 6341–6365. https://doi.org/10.5194/gmd-18-6341-2025

Mantsis, D. F., & Clement, A. C. (2009). Simulated variability in the mean atmospheric meridional circulation over the 20th century. *Geophysical Research Letters*, *36*(6). https://doi.org/10.1029/2008GL036741

Mantua, N. J., Hare, S. R., Zhang, Y., Wallace, J. M., & Francis, R. C. (1997). *A Pacific Interdecadal Climate Oscillation with Impacts on Salmon Production**. https://journals.ametsoc.org/view/journals/bams/78/6/1520-0477_1997_078_1069_apicow_2_0_co_2.xml

Marvel, K., Cook, B. I., Bonfils, C. J. W., Durack, P. J., Smerdon, J. E., & Williams, A. P. (2019). Twentieth-century hydroclimate changes consistent with human influence. *Nature*, *569*(7754), 59–65. https://doi.org/10.1038/s41586-019-1149-8

Mason, S. J., & Goddard, L. (2001). Probabilistic Precipitation Anomalies Associated with ENSO. *Bulletin of the American Meteorological Society*, *82*(4), 619–638. https://doi.org/10.1175/1520-0477(2001)082%3C0619:ppaawe%3E2.3.co;2

McCabe, G. J., Palecki, M. A., & Betancourt, J. L. (2004). Pacific and Atlantic Ocean influences on multidecadal drought frequency in the United States. *Proceedings of the National*

*Academy of Sciences of the United States of America*, *101*(12), 4136–4141. https://doi.org/10.1073/pnas.0306738101

Miralles, D. G., Bonte, O., Koppa, A., Baez-Villanueva, O. M., Tronquo, E., Zhong, F., Beck, H. E., Hulsman, P., Dorigo, W., Verhoest, N. E. C., & Haghdoost, S. (2025). GLEAM4: Global land evaporation and soil moisture dataset at 0.1° resolution from 1980 to near present. *Scientific Data*, *12*(1), 416. https://doi.org/10.1038/s41597-025-04610-y

Mishra, A. K., & Singh, V. P. (2010). A review of drought concepts. *Journal of Hydrology*, *391*(1), 202–216. https://doi.org/10.1016/j.jhydrol.2010.07.012

Mo, K. C. (2000). *Relationships between Low-Frequency Variability in the Southern Hemisphere and Sea Surface Temperature Anomalies*. https://journals.ametsoc.org/view/journals/clim/13/20/1520-0442_2000_013_3599_rblfvi_2.0.co_2.xml

Neelin, J. D., Jin, F.-F., & Syu, H.-H. (2000). *Variations in ENSO Phase Locking*. https://journals.ametsoc.org/view/journals/clim/13/14/1520-0442_2000_013_2570_viepl_2.0.co_2.xml

Newman, M., Alexander, M. A., Ault, T. R., Cobb, K. M., Deser, C., Lorenzo, E. D., Mantua, N. J., Miller, A. J., Minobe, S., Nakamura, H., Schneider, N., Vimont, D. J., Phillips, A. S., Scott, J. D., & Smith, C. A. (2016). *The Pacific Decadal Oscillation, Revisited*. https://doi.org/10.1175/JCLI-D-15-0508.1

Norel, M., Kałczyński, M., Pińskwar, I., Krawiec, K., & Kundzewicz, Z. W. (2021). Climate Variability Indices—A Guided Tour. *Geosciences*, *11*(3), 128. https://doi.org/10.3390/geosciences11030128

Özger, M., Mishra, A. K., & Singh, V. P. (2009). Low frequency drought variability associated with climate indices. *Journal of Hydrology*, *364*(1), 152–162. https://doi.org/10.1016/j.jhydrol.2008.10.018

Pendergrass, A. G., Meehl, G. A., Pulwarty, R., Hobbins, M., Hoell, A., AghaKouchak, A., Bonfils, C. J. W., Gallant, A. J. E., Hoerling, M., Hoffmann, D., Kaatz, L., Lehner, F., Llewellyn, D., Mote, P., Neale, R. B., Overpeck, J. T., Sheffield, A., Stahl, K., Svoboda, M., … Woodhouse, C. A. (2020). Flash droughts present a new challenge for subseasonal-to-seasonal prediction. *Nature Climate Change*, *10*(3), 191–199. https://doi.org/10.1038/s41558-020-0709-0

Phillips, A., Deser, C., Fasullo, J. T., Schneider, D. P., & Simpson, I. R. (2020). *Assessing Climate Variability and Change in Model Large Ensembles: A User's Guide to the "Climate*

*Variability Diagnostics Package for Large Ensembles" Version 1.0*. https://opensky.ucar.edu/islandora/object/manuscripts%3A1001

Phillips, H. E., Tandon, A., Furue, R., Hood, R., Ummenhofer, C. C., Benthuysen, J. A., Menezes, V., Hu, S., Webber, B., Sanchez-Franks, A., Cherian, D., Shroyer, E., Feng, M., Wijesekera, H., Chatterjee, A., Yu, L., Hermes, J., Murtugudde, R., Tozuka, T., … Wiggert, J. (2021). Progress in understanding of Indian Ocean circulation, variability, air–sea exchange, and impacts on biogeochemistry. *Ocean Science*, *17*(6), 1677–1751. https://doi.org/10.5194/os-17-1677-2021

Power, S., Haylock, M., Colman, R., & Wang, X. (2006). The Predictability of Interdecadal Changes in ENSO Activity and ENSO Teleconnections. *Journal of Climate*, *19*(19), 4755–4771. https://doi.org/10.1175/JCLI3868.1

Rayner, N. A., Parker, D. E., Horton, E. B., Folland, C. K., Alexander, L. V., Rowell, D. P., Kent, E. C., & Kaplan, A. (2003). Global analyses of sea surface temperature, sea ice, and night marine air temperature since the late nineteenth century. *Journal of Geophysical Research: Atmospheres*, *108*(D14), 2002JD002670. https://doi.org/10.1029/2002JD002670

Reason, C. j. c., & Rouault, M. (2002). ENSO-like decadal variability and South African rainfall. *Geophysical Research Letters*, *29*(13), 16-1-16–4. https://doi.org/10.1029/2002GL014663

Risbey, J. S., Pook, M. J., McIntosh, P. C., Wheeler, M. C., & Hendon, H. H. (2009). *On the Remote Drivers of Rainfall Variability in Australia*. https://doi.org/10.1175/2009MWR2861.1

Rodell, M., & Li, B. (2023). Changing intensity of hydroclimatic extreme events revealed by GRACE and GRACE-FO. *Nature Water*, *1*(3), 241–248. https://doi.org/10.1038/s44221-023-00040-5

Ropelewski, C. F., & Halpert, M. S. (1987). *Global and Regional Scale Precipitation Patterns Associated with the El Niño/Southern Oscillation*. https://journals.ametsoc.org/view/journals/mwre/115/8/1520-0493_1987_115_1606_garspp_2_0_co_2.xml

Saji, N. H., Goswami, B. N., Vinayachandran, P. N., & Yamagata, T. (1999). A dipole mode in the tropical Indian Ocean. *Nature*, *401*(6751), 360–363. https://doi.org/10.1038/43854

Schubert, S. D., Stewart, R. E., Wang, H., Barlow, M., Berbery, E. H., Cai, W., Hoerling, M. P., Kanikicharla, K. K., Koster, R. D., Lyon, B., Mariotti, A., Mechoso, C. R., Müller, O. V., Rodriguez-Fonseca, B., Seager, R., Seneviratne, S. I., Zhang, L., & Zhou, T. (2016). *Global*

*Meteorological Drought: A Synthesis of Current Understanding with a Focus on SST Drivers of Precipitation Deficits*. https://doi.org/10.1175/JCLI-D-15-0452.1

Schubert, S., Gutzler, D., Wang, H., Dai, A., Delworth, T., Deser, C., Findell, K., Fu, R., Higgins, W., Hoerling, M., Kirtman, B., Koster, R., Kumar, A., Legler, D., Lettenmaier, D., Lyon, B., Magana, V., Mo, K., Nigam, S., … Zeng, N. (2009). A U.S. CLIVAR Project to Assess and Compare the Responses of Global Climate Models to Drought-Related SST Forcing Patterns: Overview and Results. *Journal of Climate*, *22*(19), 5251–5272. https://doi.org/10.1175/2009JCLI3060.1

Seager, R., Harnik, N., Robinson, W. A., Kushnir, Y., Ting, M., Huang, H.-P., & Velez, J. (2005). *Mechanisms of ENSO-forcing of hemispherically symmetric precipitation variability*. *131*(608), 1501–1527. https://doi.org/10.7916/d8-8zfm-dz85

Seager, R., Henderson, N., & Cane, M. (2022). *Persistent Discrepancies between Observed and Modeled Trends in the Tropical Pacific Ocean*. https://doi.org/10.1175/JCLI-D-21-0648.1

Seager, R., Liu, H., Osborn, T. J., Kushnir, Y., Nakamura, J., & Wu, Y. (2026). Mediterranean Drying by a Positive North Atlantic Oscillation Trend over the Last 65 Years Is an Extreme Outlier in the CMIP6 Multimodel Ensemble. *Journal of Climate*, *39*(2), 785–804. https://doi.org/10.1175/JCLI-D-25-0359.1

Seager, R., Ting, M., Alexander, P., Liu, H., Nakamura, J., Li, C., & Newman, M. (2023). Ocean-forcing of cool season precipitation drives ongoing and future decadal drought in southwestern North America. *Npj Climate and Atmospheric Science*, *6*(1), 1–12. https://doi.org/10.1038/s41612-023-00461-9

Seager, R., Wu, Y., Cherchi, A., Simpson, I. R., Osborn, T. J., Kushnir, Y., Lukovic, J., Liu, H., & Nakamura, J. (2024). Recent and near-term future changes in impacts-relevant seasonal hydroclimate in the world's Mediterranean climate regions. *International Journal of Climatology*, *44*(11), 3792–3820. https://doi.org/10.1002/joc.8551

Stein, K., Timmermann, A., Schneider, N., Jin, F.-F., & Stuecker, M. F. (2014). *ENSO Seasonal Synchronization Theory*. https://doi.org/10.1175/JCLI-D-13-00525.1

Swain, D. L., Prein, A. F., Abatzoglou, J. T., Albano, C. M., Brunner, M., Diffenbaugh, N. S., Singh, D., Skinner, C. B., & Touma, D. (2025). Hydroclimate volatility on a warming Earth. *Nature Reviews Earth & Environment*, *6*(1), 35–50. https://doi.org/10.1038/s43017-024-00624-z

Taschetto, A. S., Ummenhofer, C. C., Stuecker, M. F., Dommenget, D., Ashok, K., Rodrigues, R. R., & Yeh, S.-W. (2020). ENSO Atmospheric Teleconnections. In *El Niño Southern*

*Oscillation in a Changing Climate* (pp. 309–335). American Geophysical Union (AGU). https://doi.org/10.1002/9781119548164.ch14

Tedeschi, R. G., Cavalcanti, I. F. A., & Grimm, A. M. (2013). Influences of two types of ENSO on South American precipitation. *International Journal of Climatology*, *33*(6), 1382–1400. https://doi.org/10.1002/joc.3519

Thompson, D. W. J., & Wallace, J. M. (1998). The Arctic oscillation signature in the wintertime geopotential height and temperature fields. *Geophysical Research Letters*, *25*(9), 1297–1300. https://doi.org/10.1029/98GL00950

Thompson, D. W. J., & Wallace, J. M. (2000). *Annular Modes in the Extratropical Circulation. Part I: Month-to-Month Variability*. https://journals.ametsoc.org/view/journals/clim/13/5/1520-0442_2000_013_1000_amitec_2.0.co_2.xml

Thornton, P. K., Ericksen, P. J., Herrero, M., & Challinor, A. J. (2014). Climate variability and vulnerability to climate change: A review. *Global Change Biology*, *20*(11), 3313–3328. https://doi.org/10.1111/gcb.12581

Ting, M., Kushnir, Y., Seager, R., & Li, C. (2011). Robust features of Atlantic multi-decadal variability and its climate impacts. *Geophysical Research Letters*, *38*(17). https://doi.org/10.1029/2011GL048712

Trenberth, K. E. (1997). *The Definition of El Niño*. https://journals.ametsoc.org/view/journals/bams/78/12/1520-0477_1997_078_2771_tdoeno_2_0_co_2.xml

Trenberth, K. E., Branstator, G. W., Karoly, D., Kumar, A., Lau, N.-C., & Ropelewski, C. (1998). Progress during TOGA in understanding and modeling global teleconnections associated with tropical sea surface temperatures. *Journal of Geophysical Research: Oceans*, *103*(C7), 14291–14324. https://doi.org/10.1029/97JC01444

Trenberth, K. E., Dai, A., van der Schrier, G., Jones, P. D., Barichivich, J., Briffa, K. R., & Sheffield, J. (2014). Global warming and changes in drought. *Nature Clim Change*, *4*(1), 17–22. https://doi.org/10.1038/nclimate2067

Trenberth, K. E., & Hurrell, J. W. (1994). *Decadal atmosphere-ocean variations in the Pacific*.

Ummenhofer, C. C., Gupta, A. S., Briggs, P. R., England, M. H., McIntosh, P. C., Meyers, G. A., Pook, M. J., Raupach, M. R., & Risbey, J. S. (2011). *Indian and Pacific Ocean Influences on Southeast Australian Drought and Soil Moisture*. https://doi.org/10.1175/2010JCLI3475.1

van der Schrier, G., Barichivich, J., Briffa, K. R., & Jones, P. D. (2013). A scPDSI-based global data set of dry and wet spells for 1901–2009. *Journal of Geophysical Research: Atmospheres*, *118*(10), 4025–4048. https://doi.org/10.1002/jgrd.50355

van der Schrier, G., Jones, P. D., & Briffa, K. R. (2011). The sensitivity of the PDSI to the Thornthwaite and Penman-Monteith parameterizations for potential evapotranspiration. *Journal of Geophysical Research: Atmospheres*, *116*(D3). https://doi.org/10.1029/2010JD015001

Villafuerte, M. Q., & Matsumoto, J. (2015). Significant Influences of Global Mean Temperature and ENSO on Extreme Rainfall in Southeast Asia. *Journal of Climate*, *28*(5), 1905–1919. https://doi.org/10.1175/JCLI-D-14-00531.1

Wang, B., Wu, R., & Fu, X. (2000). *Pacific–East Asian Teleconnection: How Does ENSO Affect East Asian Climate?* https://journals.ametsoc.org/view/journals/clim/13/9/1520-0442_2000_013_1517_peathd_2.0.co_2.xml

Williams, A. P., Cook, B. I., & Smerdon, J. E. (2022). Rapid intensification of the emerging southwestern North American megadrought in 2020–2021. *Nature Climate Change*, *12*(3), 232–234. https://doi.org/10.1038/s41558-022-01290-z

Williams, A. P., Cook, E. R., Smerdon, J. E., Cook, B. I., Abatzoglou, J. T., Bolles, K., Baek, S. H., Badger, A. M., & Livneh, B. (2020). Large contribution from anthropogenic warming to an emerging North American megadrought. *Science*, *368*(6488), 314–318. https://doi.org/10.1126/science.aaz9600

Wills, R. C., Schneider, T., Wallace, J. M., Battisti, D. S., & Hartmann, D. L. (2018). Disentangling Global Warming, Multidecadal Variability, and El Niño in Pacific Temperatures. *Geophysical Research Letters*, *45*(5), 2487–2496. https://doi.org/10.1002/2017GL076327

WMO. (2023). *State of Global Water Resources 2023*. United Nations.

Yeh, S.-W., Cai, W., Min, S.-K., McPhaden, M. J., Dommenget, D., Dewitte, B., Collins, M., Ashok, K., An, S.-I., Yim, B.-Y., & Kug, J.-S. (2018). ENSO Atmospheric Teleconnections and Their Response to Greenhouse Gas Forcing. *Reviews of Geophysics*, *56*(1), 185–206. https://doi.org/10.1002/2017RG000568

Yuan, X., Wang, L., Wu, P., Ji, P., Sheffield, J., & Zhang, M. (2019). Anthropogenic shift towards higher risk of flash drought over China. *Nature Communications*, *10*(1), 4661. https://doi.org/10.1038/s41467-019-12692-7

Yuan, X., Wang, Y., Ji, P., Wu, P., Sheffield, J., & Otkin, J. A. (2023). A global transition to flash droughts under climate change. *Science*, *380*(6641), 187–191. https://doi.org/10.1126/science.abn6301

Zhang, R., & Delworth, T. L. (2006). Impact of Atlantic multidecadal oscillations on India/Sahel rainfall and Atlantic hurricanes. *Geophysical Research Letters*, *33*(17). https://doi.org/10.1029/2006GL026267

Zhang, R., Sutton, R., Danabasoglu, G., Kwon, Y.-O., Marsh, R., Yeager, S. G., Amrhein, D. E., & Little, C. M. (2019). A Review of the Role of the Atlantic Meridional Overturning Circulation in Atlantic Multidecadal Variability and Associated Climate Impacts. *Reviews of Geophysics*, *57*(2), 316–375. https://doi.org/10.1029/2019RG000644

Zhang, S., Zhou, L., Zhang, L., Yang, Y., Wei, Z., Zhou, S., Yang, D., Yang, X., Wu, X., Zhang, Y., Li, X., & Dai, Y. (2022). Reconciling disagreement on global river flood changes in a warming climate. *Nature Climate Change*, *12*(12), 1160–1167. https://doi.org/10.1038/s41558-022-01539-7

Zhao, M., A, G., Liu, Y., & Konings, A. G. (2022). Evapotranspiration frequently increases during droughts. *Nature Climate Change*, *12*(11), 1024–1030. https://doi.org/10.1038/s41558-022-01505-3

## Supplementary Files

This is a list of supplementary files associated with this preprint. Click to download.

- HYDRASupplement.pdf